Factors controlling and influencing polymorphism, morphology and size of calcium carbonate synthesized through the carbonation route: A review

Powder Technology 398 (2022) 117050

Contents lists available at ScienceDirect

Powder Technology

journal homepage: www.elsevier.com/locate/powtec

Review

Factors controlling and influencing polymorphism, morphology and size of calcium carbonate synthesized through the carbonation route: A review

Freddy Liendo, Mara Arduino, Fabio A. Deorsola *, Samir Bensaid

Department of Applied Science and Technology, Politecnico di Torino, Corso Duca degli Abruzzi, 24, 10129 Torino, Italy

ARTICLE INFO

Article history:
Received 11 June 2021
Received in revised form 17 November 2021
Accepted 1 December 2021
Available online 8 December 2021

Keywords:
Carbonation
CO_2
Calcite
Aragonite
Vaterite
Control size
Synthesis

ABSTRACT

$CaCO_3$ particles are widely employed in different fields due to their properties, such as tunable size and morphology, tailored porosity and surface area, biocompatibility and nontoxicity. Therefore, many researchers have studied and developed several synthesis methods, even with and without additives. Among them, the synthesis of $CaCO_3$ through the carbonation method can be considered the most eco-friendly and innovative one. A continuously growing research effort has been devoted to this method since it could represent a potential process for CO_2 mitigation. Furthermore, this method could involve the use of several wastes as raw inputs, such as flue gases, distiller waste, steel converter slag, oil shale ash, waste concrete, etc., which would reduce the environmental impact of the process. This review article is mainly focused on this approach and the process parameters that affect the yield, particle size, morphology and crystalline phase. The control of size and morphology through different experimental setups and the use of additives is also described. Furthermore, the current uses of $CaCO_3$ in different fields, such as material filling, papermaking, medicine and personal care, are discussed, and its role in these applications is reported.

Contents

* Corresponding author.
E-mail address: fabio.deorsola@polito.it (F.A. Deorsola).

https://doi.org/10.1016/j.powtec.2021.117050

1. Introduction

Nano and micro materials are widely used nowadays due to their properties, which can significantly improve different processes or applications. They show high surface areas and volume, which enhance mass and heat transfer and provide contact area, favouring the interaction with other compounds in order to facilitate and control chemical reactions. They can be synthesized through many routes, such as reactive precipitation, crystallization, sol-gel, hydrothermal synthesis, even microwave or ultrasound-assisted methods. The properties of these materials can be tailored according to the synthesis method. Several parameters, such as supersaturation, temperature, pH, ionic strength, stirring, etc., have substantial effects on the final properties of the material. Among the most studied materials, metal oxides, such as copper oxide, aluminium oxide, zinc oxide, metals such as gold, silver and platinum, and mineral carbonates, like magnesium and calcium carbonate, can be cited.

1.1. $CaCO_3$ overview

Precipitated Calcium Carbonate (PCC) is a widely studied material. The versatility and design of $CaCO_3$ particles have aroused considerable interest in both the scientist and the industrial community due to their wide field of applications and biocompatibility. PCC is widely used as filler in paints, pigments, plastics, fibres and cement, according to its characteristics, such as morphology and size.

$CaCO_3$ is present in nature in the forms of chalk, limestone, marble, and it is produced by the sedimentation of the shells of small fossilized snails, shellfish and coral. $CaCO_3$ exists in three different crystalline forms, which are, in the order of stability, calcite, aragonite and vaterite [1]. These crystalline phases of calcium carbonate have different crystal structures and morphologies, as illustrated in Fig. 1. Vaterite crystals have a hexagonal structure, aragonite crystals show an orthorhombic structure, while calcite crystals present a rhombohedral structure.

The mechanism of precipitation of $CaCO_3$ has been widely studied, and it is divided into three main stages: i) predominant presence of Amorphous Calcium Carbonate (ACC) nucleated at the beginning of the process; ii) dissolution of unstable ACC and recrystallization into vaterite and calcite iii) dissolution of the metastable vaterite and recrystallization into the most stable crystalline form, calcite [2–5]. However, the other polymorphic forms, vaterite and aragonite, can be formed by controlling the synthesis parameters, such as temperature, pH, saturation levels, and additives concentration [6–13]. For instance, temperatures higher than 40 °C and the addition of Mg^{2+} ions in adequate concentration generally lead to the formation of needle-like aragonite metastable particles [6–10]. This is because Mg^{2+} is incorporated into the calcite lattice but not into the lattice of aragonite, increasing the solubility of calcite and decreasing the aragonite growth [14,15]. On the other hand, vaterite could be favoured by pH lower than 12 and adequate concentrations of ammonium ions. These ions can be adsorbed on the surface of the precipitated vaterite particles and can stabilize these particles avoiding the previously described transformation into calcite [11–13]. The nucleation and growth are influenced by the saturation level determined by Eq. (1), where $a_{Ca^{2+}}$, $a_{CO3^{2-}}$ and k_{sp} are the activity coefficient of calcium ions, carbonate ions and the solubility product of the $CaCO_3$ respectively. The k_{sp} varies for each crystalline phase according to its stability, consequently it is lower for the most stable crystalline form, calcite.

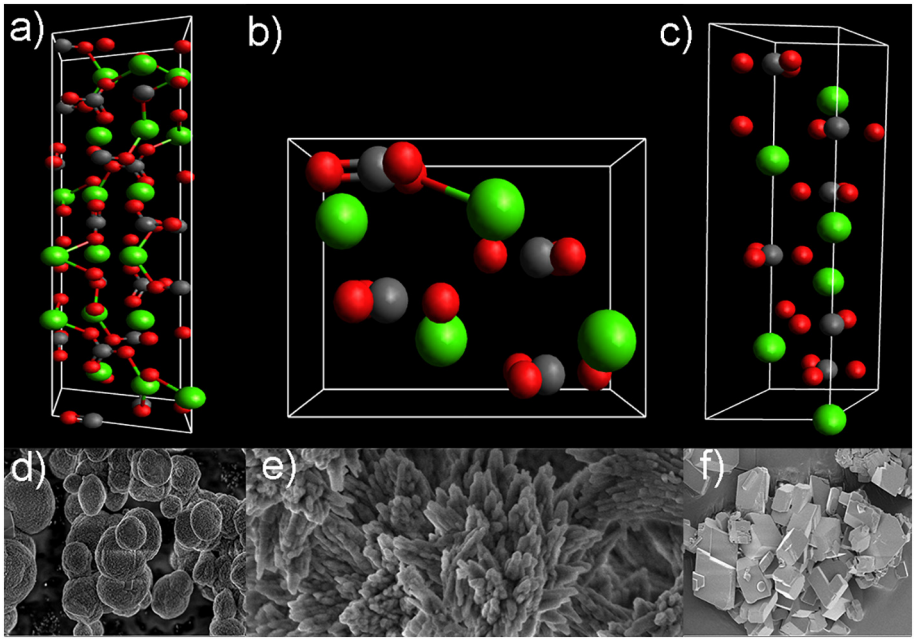

Fig. 1. Crystal structures and typical morphologies of a,d) vaterite; b,e) aragonite; c,f) calcite.

$$S = \sqrt{\frac{aCa^{2+}aCO_3^{2-}}{k_{sp}}} \quad (1)$$

1.2. $CaCO_3$ polymorph highlights and applications

$CaCO_3$ has a wide variety of applications according to the polymorphism since different properties and features characterize the various crystal phases. According to the final use of the product, different morphologies can be synthesized by varying the operating parameters, as reported in Table 1.

1.2.1. Vaterite

Vaterite is easily formed at high supersaturations, but it is metastable, and once formed, it may turn into aragonite or calcite [3,16]. However, there are several applications of $CaCO_3$ where vaterite is preferred over the other crystalline phases due to its porosity and tuneable size and morphology [17,18]. Among such applications, personal care and biomedical fields can be mentioned [17–19]. It has also been proven a beneficial effect as cement filler [20].

1.2.1.1. Personal care. Vaterite is inert and has low toxicity and good mechanical and chemical properties, making it a very interesting material for personal care applications. It improves rheology, physical robustness and visual appearance [17]. It demonstrates a good performance as abrasive, absorbent, anticaking agents, buffers, fillers colorants and emulsion stabilizers [17,21–23].

Strong demand for spherical vaterite particles has arisen in the oral hygiene field due to their excellent cleaning properties without being excessively abrasive [17,21]. The use of vaterite particles in dentifrices, teeth whitening and mouthwashes provides them cleaning and abrasive characteristics [24]. Their abrasive effect is also employed to remove paints [17].

The whiteness and absorbent properties of $CaCO_3$ particles have also been employed in several make-up and skin care cosmetics [17]. Besides, they are even employed for sunscreens fabrication because vaterite particles of a certain size can scatter UV light [21].

1.2.1.2. Biomedical applications. Nanometric vaterite is widely employed in dental care and regenerative medicine as bone cements, dental implants and scaffolds, especially because it has better mechanical strength with respect to polymers [25,26].

High porosity and surface area make it an interesting material also for drug delivery and as preservative containers since its structure provides an opportunity to absorb a large range of biomolecules [17,25,27,28]. Their properties allow the absorption of a wide range of biomolecules, especially owing to their surface morphology [17]. Besides, being added to the scaffolds, cell proliferation and differentiation towards osteoblasts are facilitated due to their micro pore structure. Moreover, vaterite in contact with body fluid dissolves immediately, supplying calcium ions, while part of it recrystallizes as the most stable phase, calcite. At the same time, the pH can be neutralized at the inflamed site of implantation by action of the released carbonate ions. Moreover, vaterite is found to co-precipitate some therapeutics, such as nucleic acids, enzymes, antibodies and proteins [17].

1.2.1.3. Filler in cement materials. Vaterite nanoparticles have exhibited a good performance as filler material in cement, even better than the calcite ones in some cases. In fact, they can enhance both the effect of the acceleration of the early age hydration of cement and the filling effects, thus increasing the final properties of the cementitious materials. In experiments carried out by Hargis et al., vaterite reduced the set time with respect to calcite, although the particle size of vaterite and calcite were different, 2 and 4.5 μm respectively [20]. The flexural and compressive strength of the cement are determined by the chemical transformations that the cement paste suffers during the ageing process. One of them is the transformation of monosulfoaluminate into monocarboaluminate [20,29]. This reaction is accelerated by employing vaterite instead of calcite, probably due to the fact that vaterite, being metastable, can dissolve and react with monosulfoaluminate to form monocarboaluminate in a faster and effective way [20].

1.2.2. Aragonite

Aragonite crystals are metastable but slightly more stable than vaterite. Aragonite is the main component of nacre and mollusc shells [30]. The classical morphology of aragonite is needle-like [19,31,32]. Nonetheless, other morphologies, such as pyramid-shaped [31], multi-layered [32], hubbard squash-like [32], pseudo hexagonal and dendrite-like, have also been synthesized. The applications of aragonite depend on the aspect ratio (length/diameter ratio) of the needle, which depends on the synthesis method and the operating parameters of the synthesis [9,30,31,33]. Among the applications of aragonite, bone regenerative medicine [34], papermaking [35,36] and filler in rubber and plastic [31] can be cited.

1.2.2.1. Regenerative medicine. Bioactive materials have the capability to create a biomimetic apatite layer in contact with bone upon implantation, which is the consequence of good tissue integration [37]. Calcium carbonate shows a good *in vitro* bioactivity which has been attributed to different factors, especially to the ability of aragonite to modulate environmental calcium ion leading to its conversion into carbonate apatite crystals under biomimetic conditions [34]. Incorporation of CO_3^{2-} ions through the substitution of phosphate groups increases the effectiveness of cell adhesion and proliferation [38], and it has an important effect on the physical and chemical properties of apatite, such as solubility and dissolution rate [34].

1.2.2.2. Papermaking. Calcium carbonate has been used as filler in alkaline papermaking for years to reduce costs and to provide desired end-use properties of paper products [35]. Although increasing the filler amount can improve certain properties like brightness, porosity, smoothness, etc., it could cause some problems, such as reduced paper strength and stiffness, increased size demand, abrasion, and dusting [6,35]. The implementation of needle-like aragonite particles can provide better properties to paper in terms of higher bulk, brightness, opacity and

Table 1
Favorable conditions for the synthesis of the different $CaCO_3$ polymorphs through the carbonation route and their main applications.

Polymorph	Stability	Operating conditions	Applications
Calcite	Most stable $CaCO_3$ polymorph at any temperature	High pH and supersaturations	• Personal care [61,63–67] • Biomedical applications [26,58,60,62,68–73] • Filler [29,55,58,74–80]
Aragonite	Metastable	Use of Mg^{2+} as additive. High temperature and low pH.	• Regenerative medicine [34,37,38] • Papermaking [6,35,39] • Filler in rubber and plastics [31,40]
Vaterite	Least stable $CaCO_3$ polymorph	Use of NH_4^+ as additive. Low supersaturation and pH.	• Personal care [17,21–24] • Biomedical applications [17,25–28] • Filler in cement materials [20,29]

strength, as well as improved retention [39]. Hu et al. tested the tensile strength and folding endurance of the paper by using commercial PCC and needle-like aragonite as filler. Samples filled with needle-like particles showed higher tensile strength and folding endurance, which suggests that this morphology is indeed able to improve paper strength [35].

1.2.2.3. Filler in rubber and plastic. Needle-like aragonite particles with a very high aspect ratio are particularly employed as filler in rubber and plastic, because they increase the bending strength of these materials. Therefore, needle-like aragonite particles are employed in car bumpers and dashboards as filler incorporated into thermoplastic and polypropylene resins [31]. Besides, whisker aragonite particles showed better performance than calcite in polyvinyl alcohol and polypropylene composites. Aragonite particles increased tensile and impact strengths of the composite, improved the glass transition temperature and the decomposition temperature [40].

1.2.3. Calcite

Calcite is the most stable polymorph of $CaCO_3$ at any temperature [1,16,41,42]. It is easily synthesizable through the carbonation route without additives or specific conditions of temperature or pressure [19]. Nonetheless, the shape and size of these particles can be tailored for specific applications by tuning the operating parameters. Lots of works have been carried out to control the morphology, obtain calcite with several morphologies, and avoid the formation of metastable phases [43–58]. The control of shape, size and biocompatibility [56,59] of calcite crystals makes them very useful for a wide range of applications, such as personal care, biomedical applications and filler [19,55,58,60–62].

1.2.3.1. Personal care. Calcite, similarly to vaterite, is used in dental care by adding it to soft drinks [61]. Khoozani et al. added calcite nanoparticles to soft drinks and determined that they can avoid or reduce tooth erosion [61] caused by eating/drinking acidic products [63]. Nanometric calcite can be employed for early caries lesions since it acts as a calcium source to retain the Ca^{2+} ions in the supersaturation state in the enamel minerals [64]. The deposition of Ca^{2+} ions on the demineralized enamel surface might support the remineralization process of the outer enamel caries lesion [65]. In fact, some researchers have added calcite microparticles (size $< 10\,\mu m$), which supports the reduction of enamel demineralization likely due to the buffering power of abrasive particles [66]. The results of Cury et al. suggest that abrasive $CaCO_3$ may enhance the effect of fluoride present in dentifrice on dental caries control [66]. High-stable spherical and porous calcite exhibits high adsorption capability for Immunoglobulin Y, thus leading to an enhanced antibacterial effect against oral bacteria [67].

1.2.3.2. Biomedical applications. Calcite particles with a hollow or porous spherical structure are useful for drug delivery and cancer treatment [58,62,68]. Drugs and protein like Doxorubicin (DOX, an anticancer agent) [68,69] Betamethasone phosphate (BP, a type of medicine used to reduce inflammation, irritation, and pain) and Erythropoietin (an essential hormone for red blood cell production) [70] can be incorporated and loaded on the surface of hollow or porous calcite or into its structure [68–70]. Calcite is also widely used in bone implants, since it bonds directly to the bone [26,60]. It is possible to form bone substitute scaffolds with controlled internal architecture through a simple slip-casting process [71]. This is because carboxylate and sulphate groups in the bone matrix can bond strongly to the exposed calcium sites of calcite to form stable calcium-carboxylate and calcium-sulphate compounds [72]. Vaterite can also be employed thanks to its spherical and porous structure, although it could degrade after three months when placed in a bone generating defect due to its instability [73].

1.2.3.3. Filler. Calcite nanoparticles have a good performance as filler in cements and enhance the flexural and compressive strength of cementitious materials [29,55,74]. The enhancement depends on the filler content and the particle size. Microsized calcite particles provide an acceleration of the hydration rate of calcium silicates, but the final properties after 28 days of curing are not improved [74]. On the other hand, nanosized calcite particles improved both the hydration rate because it acts as seeding, and the final compressive and flexural strength, since their dimension provides them the capability to fill the small cracks [74,75].

Stable calcite particles have been employed as fillers in polymers like polypropylene [76–79] and polyethylene [80]. The addition of calcite to polypropylene composites improves the wear properties of the material [77,78]. This is because the presence of crystals in semi-crystalline polymers will increase the temperature of glass transition, owing to the resistance of the crystals to the movement of polymeric molecules [78]. The effect depends on the morphology and crystal faces of calcite [79]. In the case of polyethylene, calcite particles increase the mass density of the product and improve the modulus of Young above that of the neat matrix and well above the reduced moduli of Young of the rubber-reinforced product [80]. Calcite particles with a hollow structure have been tested in vacuum insulating panels (VIPs) as core material, showing a good performance for energy saving applications. Therefore, they could be employed also as sound and heat insulating materials in paint and coating [58].

2. $CaCO_3$ synthesis methods

$CaCO_3$ can be considered easy to be synthesized, and several biomimetic methods are employed as an attempt to mimic the natural process for the synthesis of complex and elegant shapes, for example shells in marine animals [19]. Nature uses biomolecules and ions to produce nuclei, which are then transformed into various shapes.

In biomimetic methods, many additives are used (in low quantity, ppm or g/L), which do not alter the chemical properties of $CaCO_3$. The role of additives is mainly to interact with Ca^{2+}, provide active sites for the nucleation, and subsequently bond to a preferential surface by preventing or favouring the growth of $CaCO_3$ particles in specific crystallographic planes. This enables the control of the size and stabilizes different morphologies, such as spheres, hollow spheres, pyramidal particles, flower-like, laminated particles, etc. Besides, the additives can interact with the surface, potentially stabilizing metastable aragonite or vaterite particles over stable calcite particles.

The next paragraphs will describe how the size, morphology and polymorphism of $CaCO_3$ can be controlled by the synthesis method and the operating parameters, such as temperature, pH, supersaturation, etc.

2.1. Spontaneous precipitation

This method consists in the mixing of a calcium salt solution with a carbonate salt solution, as illustrated in Fig. 2a. The most used calcium salts are $CaCl_2$, $CaSO_4$ and $Ca(NO_3)_2$. On the other hand, Na_2CO_3, $(NH_4)_2CO_3$, K_2CO_3 and Mg_2CO_3 are employed as carbonate source for this synthesis method. This method can also involve the use of additives in order to favour a crystalline form over the others or to control the size or shape of the $CaCO_3$.

The most extensively studied system is the reaction between dissolved Na_2CO_3 and $CaCl_2$, which can be performed in different ways, especially by varying the addition rate of the Na_2CO_3 solution to the $CaCl_2$ one and vice versa. Many studies have demonstrated that this system generally leads to the synthesis of calcite particles, especially at high supersaturations at any temperature [81–83]. However, different strategies have been investigated to promote the formation of the vaterite and aragonite polymorphs in this system. For instance, it has been reported that the simultaneous addition of both $CaCl_2$ and Na_2CO_3 solutions could stabilize the abovementioned polymorphs [16,84]. Moreover, low levels of pH and saturation gave rise to the formation of vaterite and aragonite [81,83].

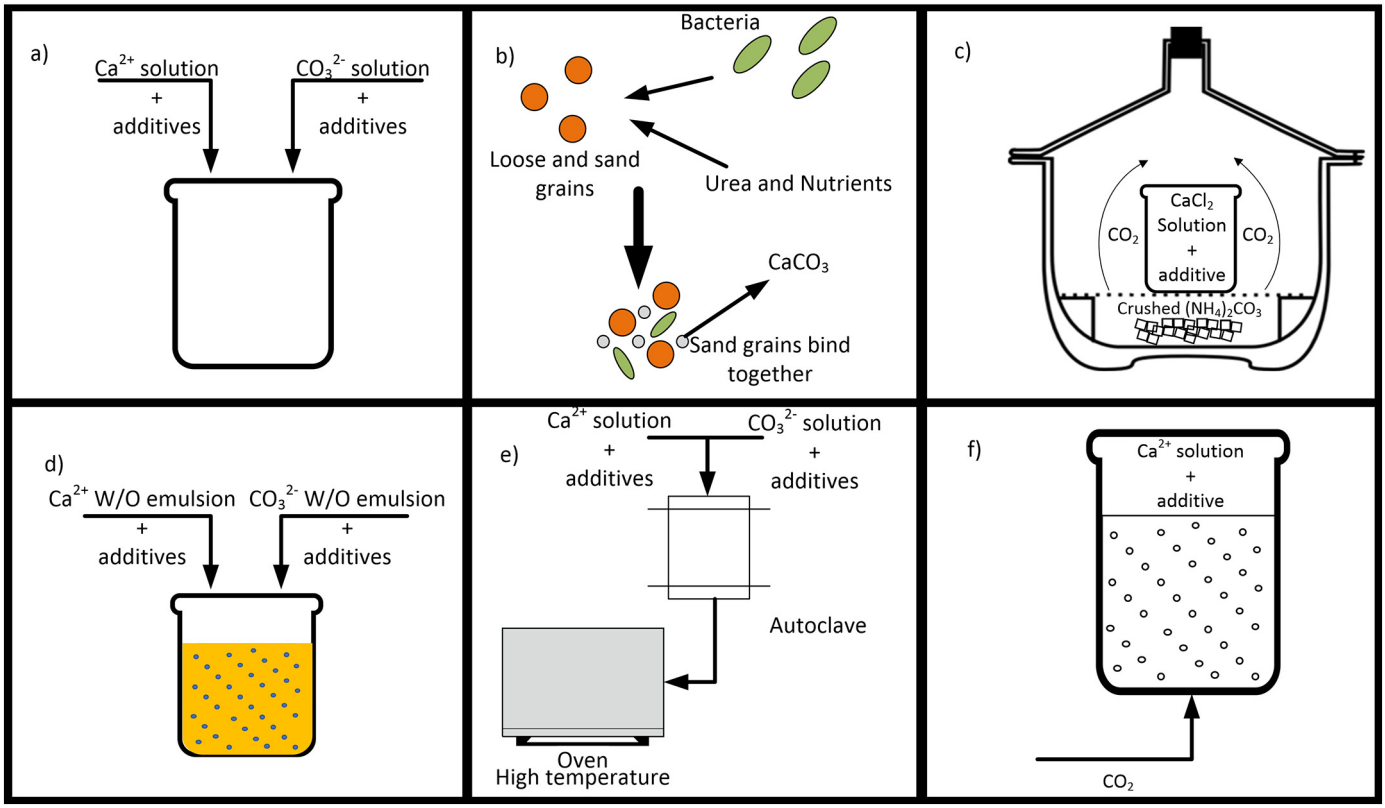

Fig. 2. Different $CaCO_3$ synthesis methods. a) spontaneous reaction. b) Microbial induced calcite precipitation. c) Slow carbonation. d) Reverse (W/O) emulsion. e) Hydrotherml synthesis f) Bubbling method. Figure modified from manuscript published by Boyjoo et al. [19].

The formation of aragonite in this system is also clearly favoured by employing high temperatures (>40 °C) and adequate concentrations of magnesium-based additives [16,83,85,86]. On the other hand, additives such as ethylene glycol (EG) and KH_2PO_4 have been employed to enhance the formation of vaterite [18] and calcite [83], respectively. The use of ultrasounds has also favored forming aragonite crystals by starting from Na_2CO_3 and $CaCl_2$ [87]. While, the formation of mainly vaterite particles was favored by substituting Na_2CO_3 with $NaHCO_3$ [82].

Different sources of carbonate ions, such as NH_4HCO_3, K_2CO_3 and $MgCO_3$ are also employed. According to Hu et al., who synthesized $CaCO_3$ starting from NH_4HCO_3 and $CaCl_2$ solutions, the presence of NH_4^+ ions created an interaction onto the surface of the vaterite particles that stabilizes them and favours its formation [12]. A similar system was studied by employing $(NH_4)_2CO_3$ and led to vaterite and calcite formation according to the Ca^{2+}/CO_3^{2-} molar ratio (R). High R values promoted the vaterite transition phase to calcite, while low values, which means high NH_4^+ ion concentrations, stabilized vaterite crystals avoiding the phase transition into calcite [88]. Chang et al. performed some experiments at 25 °C by using K_2CO_3 as carbonate source and determined that at high pH values, the formation of vaterite was fostered, while at low pH values, the calcite content was increased up to 35% and by increasing the temperature up to 50 and 80 °C mainly aragonite was obtained [8]. The use of $MgCO_3$ as carbonate ions source enhanced the formation of aragonite over any crystalline phase [6]. Different Ca^{2+} sources, such as $Ca(NO_3)$, $Ca(OH)_2$ and $CaSO_4$ were also employed in the synthesis of $CaCO_3$ particles, which led to the synthesis of aragonite particles [6,10].

In addition, ammonium carbamate [89] and urea [90] have been used as sources of carbonate ions, as these compounds hydrolyze in an aqueous solution to form ammonium carbonate, which subsequently can react with calcium ions to form precipitated calcium carbonate [91]. The concentration of urea and carbamate is determinant in the definition of the final crystal phase and morphology of $CaCO_3$. Prah et al. proved that by this precipitation route, calcium carbonate is first formed as an amorphous phase, which then transforms into a crystalline phase [89]. They investigated the effect of the temperature and the initial concentration of the reactants on the crystal morphology and structure by employing calcium acetate and ammonium carbamate in a stoichiometric ratio. They observed that calcite was formed at low concentrations of the reactants through the transformation of unstable phases, ACC, vaterite and aragonite, into stable calcite. Instead, vaterite was stabilized at high concentrations avoiding the calcite formation via vaterite. The temperature did not significantly affect the crystal phase, but the crystal size was reduced with its increase. Nan et al. studied the precipitation process by mixing a calcium dodecyl sulfate solution (44 mmol/L) with a urea solution with different concentrations [90]. Subsequently, the resulting solution was placed in an autoclave at 120 °C for 24 h. They exploited the benefits of hydrothermal synthesis, which will be discussed subsequently [90]. They observed that by increasing the urea concentration, the morphology changed from tabular sphere-shaped vaterite into bicone-shaped calcite. They attributed the polymorphic selectivity to the synergistic effects of the concentration of CO_3^{2-}, the pH value, the amount of anionic dodecyl sulfate and the presence of NH_4^+ ions [90].

Dimethyl carbonate (DMC) has also been employed as a CO_2 precursor in the solution. This is possible due to the base-catalyzed hydrolysis of the DMC, forming CO_2 in the solution and avoiding the gas-liquid interface. It has been reported by Gorna et al. that ACC precipitates in a very reproducible way as monodisperse spherical particles of sub-micrometer diameter [92]. They controlled the nucleation of ACC by varying the $CaCl_2$ concentration and pH (NaOH concentration), aiming at a narrow PSD ranging between 0.4 and 1.2 μm [92]. Dietzsch et al. studied the $CaCO_3$ crystallization mechanism in the presence or absence of polyelectrolytes, like Na-PMA, as additives. Without their

presence, they observed the classical calcite crystallization via vaterite from ACC formed through a first heterogeneous nucleation process at the air-water and air-vessel interface, followed by a second homogeneous nucleation process in solution. On the other hand, the heterogeneous nucleation step was suppressed in the presence of polyelectrolytes [93]. These results were similar to those obtained by Huber and coworkers [94]. This method has also been employed to produce cellulose-PCC composites in the presence of cellulose microfibrils, controlling the crystallization methods and modifying the crystallization mechanism to lead to the crystallization of aragonite crystals [95]. These composites could provide some advantages to the pulp and paper industry, reducing costs, increasing paper strength and provide enhanced filler retention [95].

2.2. Microbially induced calcite precipitation

Urea hydrolysis was also exploited to synthesize $CaCO_3$ through biomineralization induced by bacteria with high urease activity. The Microbially induced calcite precipitation (MICP) process is described in Fig. 2b. Urease plays an important role in urea hydrolysis. This method has been employed by several researchers [96–99]. This novel method is very attractive, as controlling the process parameters (pH, bacteria type and concentration, and calcium and urea concentration) allows the synthesis of $CaCO_3$ with different crystal morphologies and phases. Thus it can be used in several applications, such as heavy metal removal from the environment, bioconsolidation of soil and sand, biocementation and CO_2 sequestration. Gorospe et al. controlled the crystal phase by using different calcium sources, like calcium chloride, calcium acetate, calcium lactate and calcium gluconate. Literature reviews concerning the most important factors affecting the MICP process were published by Anbu et al. [96] and Krajewska [98].

2.3. Slow carbonation method

This method consists in spontaneous precipitation, where CO_3^{2-} ions are produced from the dissolution of the CO_2 gas in an alkaline solution. The CO_2 is formed via slow hydrolysis of an additive, typically $(NH_4)_2CO_3$ [19]. Generally, a $CaCl_2$ solution, with or without additives, is introduced in a desiccator, where crushed $(NH_4)_2CO_3$ is also placed. The $(NH_4)_2CO_3$ releases NH_3 and CO_2, which are consecutively absorbed in the calcium solution, and the $CaCO_3$ formation takes place as illustrated in Fig. 2c. Several researchers have studied this method for the synthesis of $CaCO_3$ [14,100–103].

Xu et al. employed this method to synthesize hollow spherical ACC stabilized by phytic acid [100]. The ACC was obtained by increasing the phytic acid concentration in the $CaCl_2$ aqueous solution, despite its instability. On the other hand, rhombohedral calcite was observed in the absence of any additive [100]. Ajikumar et al. studied a very similar system but adding different amounts of 0.75 mol/L $MgCl_2$ to change the Ca^{2+}/Mg^{2+} ratio (1:0, 1:3, 1:6 and 1:9 ratios were employed). Ajikumar and coworkers [101] obtained rhombohedral calcite without additives, as Xu et al. [100]. Instead, by increasing the $MgCl_2$ concentration (1:3 ratio), spherical calcite was obtained, and further addition of $MgCl_2$ led to the dense spherical ACC stabilization [101].

Guo et al. explored the synergistic effect of PEG-b-pGlu (synthetic polymer) and the solvent mixture on the growth of calcium carbonate by employing this method and they obtained stabilized vaterite with several structures [102]. Mixtures of N,N-dimethylformamide (DMF), and other solvents, such as THF, n-propanol, ethanol, and 1,4-dioxane, were applied. In the presence of pure DMF, the main crystal phase was calcite, but by mixing it with nonionic water (NIW), vaterite was stabilized [102]. DMF:THF and DMF:methanol mixtures promoted the precipitation of rhombohedral calcite, DMF:propanol and DMF:ethanol mixtures promoted the synthesis of spherical vaterite particles, while multibranched hierarchical structures were achieved by employing DMF:1,4 dioxane [102]. Xu et al. [103] also experimented this method by employing poly(styrene-alt-maleic acid) as an additive and obtained calcite mesocrystals with hierarchical pyramidal self-similar morphology associated with self-similar growth.

More recently, Harris and Wolf [14] synthesized $CaCO_3$ particles through this method by employing a $CaCl_2$ aqueous solution with $MgCl_2$ as an additive and studied the effect of the desiccator volume. This parameter had not been evaluated before. The Ca^{2+}/Mg^{2+} ratio employed was 1:10, and three different volumes, 21, 11.5, and 3 dm^3, so-called large, medium, and small desiccator, respectively, were considered. The crystals formed at the gas-liquid interface by using a glass slide were characterized. Thus, it was possible to observe that with large desiccators, aragonite crystals were formed at the gas-liquid interface, as expected due to the presence of magnesium. This effect was not evident in medium and small desiccators, as ACC with not-defined shape and hexagonally-packed spherical ACC crystals were formed, respectively [14]. Further studies without the presence of $MgCl_2$ led to the synthesis of a mixture of calcite and vaterite crystals in the small, medium, and large desiccators, similarly to those obtained by Xu et al. [100] and Ajikumar et al. [101]. These studies indicate that the effect of an additive on the polymorphism of the crystals synthesized through this method is strongly dependent on the size of the desiccator.

2.4. Reverse emulsion

The reverse emulsion is a thermodynamic dispersion of water and oil channels stabilized by interfacial layers of surfactants with or without co-surfactants and consisting of bi-continuous microstructures, which can be used as "micro-reactors" (see Fig. 2d) and templates for preparing nanomaterials [19]. The confinement of reagents in the aqueous droplets and the adsorption of surface-active agents on the growing crystals through the implementation of this method allows the simultaneous control of the mesoscale crystal surface and the intrinsic morphology [104]. Hence, the most important factors that affect this method have been widely studied by several researchers [104–112].

Thachepan et al. [105] investigated this approach by involving the encapsulation of a soluble crystallization inhibitor (sodium polyphosphate) into the water droplets of a reverse microemulsion prepared by mixing sodium carbonate-containing NaAOT microemulsions (water/surfactant molar ratio, w, equal to 10) with an isooctane suspension of $Ca(AOT)_2$ reverse micelles. They determined that sodium polyphosphate influenced the polymorphism and morphology of the precipitate since the crystallization process is determined by the surface adsorption of the polyphosphate ions, particularly on the vaterite crystals. Hence, increasing the additive concentration from 0 to 1 g/L passed from the synthesis of aragonite to aragonite-calcite mixture and pure vaterite at the highest additive concentration [105]. Other microemulsion attempts to synthesize $CaCO_3$ have been conducted, for instance, from oil-rich water/CTAB/1-pentanol/cyclohexane microemulsions, which can mediate a well-defined condition for hexagonal vaterite crystal growth and its conversion to more stable prismatic calcite after several days [104]. Tai and Chen [106] mixed $CaCl_2$ and Na_2CO_3 AOT/isooctane/water microemulsions by employing several water/surfactant molar ratios ($w = 5$–16), water/oil molar ratio (WOR), and R ratio. They reported that the R ratio is the main determinant factor in crystal size and habit. The w value greatly influenced the particle size and habit of calcium carbonate because it strongly affected the stability and size of aqueous droplets. For example, the particle shape changed from spherule to disk and then to irregular shape by increasing the w ratio [106].

Furthermore, other additives, such as potato starch, Fe and Cu^{2+} ions, etc., in the microemulsions can also direct the precipitation in another way. Thus, tailoring the crystal size and habit, even nanosized particles with different morphologies can be obtained [106,107]. As previously reported, several surfactants can be employed. Even polymeric surfactants have been investigated, which could form a complex

that stabilizes ACC through preferential adsorption of the polymer on its surface, blocking further growth and preventing any phase transformation to a metastable or stable phase [108].

The reverse emulsion method has also been employed to prepare hybrid nanocomposites and hybrid polymeric particles with various $CaCO_3$ nanoparticles, which were synthesized through a mini emulsion technique using 2-hydroxyethyl methacrylate (HEMA) monomer, able to induce the formation of rod-like stable calcite nanoparticles [109,110].

The use of unconventional techniques like ultrasonic cavitation was also tested to promote the synthesis of nanoparticles, e.g. Fukui and Fujimoto [109,110] employed this technique, which favored the synthesis of nanoparticles, as Badnore and Pandit did [111]. Ultrasonic cavitation favors the production of smaller droplets than conventional mechanical stirring, which results in smaller particles with a narrower Particle Size Distribution (PSD) [108,111]. Besides, ultrasounds favor the crystalline phases of $CaCO_3$ over ACC [111].

2.5. Hydrothermal and solvothermal synthesis

The hydrothermal method consists of heterogeneous reactions for the synthesis of inorganic materials in aqueous media above ambient temperature and pressure. Practically, one of more precursors are placed in a sealed stainless steel autoclave and heated above the water boiling point, generating a dramatic increase in pressure [113]. The precursors mixture is maintained under such conditions for several hours, which allow the production of highly crystalline materials (see Fig. 2e). Solvothermal synthesis is similar to the hydrothermal method, but the solvent consists of an organic solvent mixture. These methods have been employed to synthesize several nanomaterials, including ceramic materials. Rarely, $CaCO_3$ crystals have been synthesized through this method [114–118]. Mainly calcite crystals, with a low content of the vaterite and aragonite polymorphs, have been obtained with this method; nonetheless, the size and morphology of the product were successfully modified by using surfactants and varying the process parameters.

$(NH_4)_2CO_3$ and $CaCl_2$ were employed as precursors in an aqueous solution without surfactants at 200 °C by Sulimai et al., obtaining mainly calcite crystals with vaterite presence [114]. On the other hand, Zhao et al. synthesized $CaCO_3$ crystals with controlled morphology by employing CaO in Oleic Acid (OA)/ethanol as well as OA/Ethylene glycol (EG) mixtures at different temperatures (160-200-240 °C). The temperature variation and the use of different surfactants – cetyltrimethylammonium bromide (CTAB), sodium dodecyl sulfate (SDS), poly N-vinyl-2-pyrrolidone (PVP) and polyethylene glycol (PEG) – led to the synthesis of calcite crystals [115]. Nonetheless, the XRD spectra of the synthesized $CaCO_3$ showed different signal intensities for the crystalline planes, thus indicating that the morphology of the crystals was modified [115].

Other studies involved the use of these surfactants in different mixtures. Chen et al. employed PVP as a surfactant with $Ca(CH_3COO)_2$ and $CO(NH_2)_2$ as reactants in a diethylene glycol (DEG)/water mixture [116]. They obtained structured microspheres mainly formed by primary calcite nanocrystals (50-100 nm), pointing out their agglomeration. They also observed the presence of aragonite crystals. Otherwise, Ranjbar and Taher used SDS as a surfactant at 200 °C starting from a $Ca(NO_3)_2 \cdot H_2O$ aqueous solution in molar stoichiometric ratio to carbonate ions, reducing the crystal size and agglomeration of calcite crystals by increasing the synthesis time [117].

A novel microwave-assisted hydrothermal method was employed by Zieba et al. [118]. They performed the synthesis starting from a mixture of $CaCl_2$ and Na_2CO_3 in a molar ratio of 1:1 at 180 °C and 90 atm. They previously mixed the starting mixture of reactants through mechanochemical process in a planetary mill at 500 rpm in dry state for 30 min for its initial activation before the next microwave-assisted hydrothermal treatment (MWT). The MWT was conducted in saturated vapor or under a layer of water, thus modifying the porous structure of the calcite crystals. In the saturated water vapor, the crystal size was reduced and particles showed well-defined edges, while under the layer of liquid they obtained larger crystals with smoothed edges.

2.6. CO_2 bubbling methods – carbonation

The carbonation method consists in a gaseous CO_2 stream reaction with a calcium alkaline solution, as shown in Fig. 2f. Several researchers have explored the carbonation method to synthesize $CaCO_3$ and precipitation mechanism for years. The work carried out by Juvekar and Sharma [119] can be cited among the first studies dated to 70s, where the CO_2 absorption in a lime suspension was studied. This process was already employed at the industrial stage for the production of $CaCO_3$. Still, knowledge on its mechanism was lacking and not enough reliable data were present in the literature at that time [119]. Thus, they studied the process from the absorption of the CO_2 bubble to the precipitation of $CaCO_3$, by employing a bubble column as gas-liquid contactor [119]. However, several technologies and types of reactor have been explored and are still under investigation in order to maximize the performance of the process nowadays [9,19,46,120–123]. Many factors, such as additives, reactor or operating conditions, can influence and tailor the final properties of the product [9,123,124] and they will be discussed in detail in the next sections.

3. Synthesis of $CaCO_3$ through carbonation

Although the production of $CaCO_3$ is already an industrialized process, many researchers are still studying this process to assess different routes by involving waste conversion, obtain higher CO_2 conversions and achieve an intensification of the process, which could provide better control on the final properties of the particles.

3.1. Carbonation as an alternative for CO_2 mitigation

Nowadays, CO2 mitigation represents a big challenge to which a great research effort is devoted. Carbonation seems to be a successful approach thanks to its long-term storage of carbon dioxide deriving from industrial gaseous streams. Different reagents can be used to obtain $CaCO_3$ particles through carbonation. Mainly $Ca(OH)_2$ or CaO slurry are used as sources of Ca^{2+} ions [31,51,52,62], but also $CaCl_2$ and $CaSO_4$ coupled with a suitable alkalinity source are frequently used in the $CaCO_3$ precipitation reaction [44,125].

Some Life Cycle Assessment (LCA) regarding the synthesis of $CaCO_3$ through carbonation are present in literature [126,127], and some others concern mineral carbonation, which involves minerals rich in calcium and magnesium, like wollastonite and serpentine [128–132]. Moreover, these studies assess the process considering raw material wastes coming from other processes, such as steel converter and phosphogypsum desulfurization, which present a high carbonate-free calcium content in form of CaO and $Ca(OH)_2$ [126,133].

Mattila et al. suggested that if industrial wastes, like slag and CO_2, are available, it is environmentally beneficial to use them to produce precipitated $CaCO_3$. This approach saves natural resources as limestone, reduces energy consumptions and overall CO_2 emissions [126]. Zakuciová et al. also concluded that the production of $CaCO_3$ through the calcium loop reduces the CO_2 emissions in the flue gases [127].

Since 1990s, mineral carbonation has been the main carbonation method to produce mineral carbonates. This process involves the reaction between CO_2 and alkaline earth metals, present in naturally occurring silicate minerals. The mineral carbonation can be carried out either *in situ*, by injecting CO_2 in silicate-rich geological formations, alkaline aquifers, or *ex situ*, occurring above ground in a chemical processing plant. Because of the low natural abundance of calcium oxide and hydroxide, the *ex situ* carbonation requires a pretreatment step for the

extraction of the metal oxides from the silicate rocks, which are relatively abundant over the world [129,130,134]. For this reason, silicate minerals such as olivine, serpentine, dolomite and wollastonite, are considered attractive feedstocks of calcium. Even though wollastonite and dolomite minerals present higher content of calcium oxide, their relative abundance is low, so olivine and serpentine are the most frequently used silicates in *ex situ* carbonation [129].

However, the use of natural silicate rocks requires energy-intensive processes including mining, transport and grinding. Therefore, more recently, numerous studies have been carried out to use calcium-containing industrial waste, such as steel slag, bottom ash from municipal solid waste, oil shale ash, waste concrete, cement kiln dust, and brines [135].

Moreover, gypsum deriving from the desulfurization of flue gas was used by Song et al. to obtain calcite or vaterite particles by carbonation in an aqueous ammonia solution [136]. Another material that can be used to produce PCC is dolomite, $CaMg(CO_3)_2$, which provides a Ca-Mg-rich solution after a leaching process. Altiner et al. successfully synthesized pure aragonite crystals in the reaction temperature range of 40–70 °C [33].

Finally, seawater and brines from desalination processes are reported as calcium ion sources. In the first case, seawater and cement kiln dust (CKD), an alkali industrial by-product, was employed in the carbonation process, exploiting a double effect both as calcium feedstock and as a solvent for Ca elution from CKD [137]. In the second case, brine collected from a seawater reverse osmosis process for industrial water supply was employed for CO_2 mineralization [138].

Another interesting waste is the calcium-rich brine, called post-distillation liquid, deriving from the Solvay process, responsible for the salinity of the surrounding soil and groundwater. This waste contains approximately a concentration of $CaCl_2$ equal to 1 mol/L, with the presence of other ions, such as SO_4^{2-}, Mg^{2+}, etc. The carbonation of this waste could be an interesting approach to produce precipitated $CaCO_3$ in the waste management framework. This process is currently being studied by several researchers, exploring its feasibility [81,139,140]. Czaplicka et al. studied the influence of selected CO_2 absorption promoters on the characteristics of the $CaCO_3$, obtaining agglomerates of mixed vaterite and calcite polymorphs with micrometric dimensions [140].

Nonetheless, the control of the properties of the product still represents a challenge due to the high concentration of foreign ions that can affect the crystallization process. The yield of calcium carbonate precipitation in a gas-liquid system mainly depends on the ratio between the concentrations of Ca^{2+} and promoter [140]. As high as the promoter concentration is, the higher the CO_2 absorption capacity will be, so the reaction with calcium ions could occur according to the mechanism described in the following section.

3.2. H_2O-CO_2-Ca^{2+} system description

It is fundamental to understand the interaction among the main compounds involved in the carbonation process, that is the H_2O-CO_2-Ca^{2+} system, as illustrated in Eqs. (2) to (22). First, the absorption of the CO_2, which is thermodynamically limited by pressure and temperature, must be considered. The rate of absorption depends on the liquid-gas contact surface area (a) and the mass transfer coefficient (K_L), which is determined by the flow regime [119]. Afterwards, the process breakthrough to the conversion of CO_2 to carbonic acid by reaction with water and its subsequent dissociation into bicarbonate and carbonate ions due to the interaction with H^+ and OH^- (see Eqs. (2)–(6)). The concentration of H^+ could be related to the presence in solution of acids that can be used as calcium extraction agents [130,141,142]. Strong acids such as HCl, H_2SO_4 and HNO_3 completely dissociate into H^+ and X^- ions, while the dissociation of weak acid, such as HCOOH and CH_3COOH, is determined by the acid dissociation constant K_a, as in Eq. (7). The concentration of OH^- depends on the $Ca(OH)_2$ concentration or on the concentration of the absorption promoter, such as NaOH, $Mg(OH)_2$, KOH, NH_3 and amines. Because NaOH and KOH are strong bases, they dissociate completely, therefore the concentration of OH^- in solution equals the base concentration. Conversely NH_3, amines and $Mg(OH)_2$ are weak bases, so the OH^- concentration varies according to their basicity (K_b) (see Eq. (8)) [122,143–145]. Higher concentrations of OH^- enhances the CO_2 absorption. Thus, the transformation of CO_2 into the ionic species is boosted since the equilibrium is shifted to the formation of CO_3^{2-} ions. Finally, once the CO_3^{2-} ions are formed, they react with the Ca^{2+} ions, producing the precipitation of $CaCO_3$ induced by the supersaturation. When amines are used as absorption promoters, the carbonation process takes place according to the pathway described from Eqs. (17) to (22). So, it is given by the formation of zwitterion and carbamate from the reaction of the dissolved CO_2 with the amine. Zwitterion and carbamate ion undergo deprotonation by the amine. Subsequently, the deprotonated product is hydrated to form HCO_3^- ions, which react afterwards according to the previously described mechanism. The value of the equilibrium constants of Eqs. (17)–(22) will depends on the employed amine.

The precipitation process depends on the solubility product of the different $CaCO_3$ phases summarized in Eq. (16) (ACC, vaterite, aragonite and calcite). The crystallization is also influenced by the $CaCO_3^0$ formation, described in Eq. (11), which could favor the crystal growth of the $CaCO_3$ [146]. Furthermore, the reactions involving the formation of $CaOH^+$ and $CaHO_3^+$ ions, highlighted in Eqs. (9) and (10), could affect the $CaCO_3$ crystallization, especially the growth mechanism interacting with the crystal surface. Nonetheless, many researchers do not consider them in numerical calculations since the low values of the equilibrium constants indicate that their formation is not favored, and their concentration can be negligible for the ionic balance [147–149]. Instead, ions such as Cl^-, SO_4^{2-}, provided by the calcium source and ions like Na^+, K^+, NH_4^+, etc., provided by other absorption promoters, generate an interaction with the whole process according to Eqs. (12), (13) and (14), which could not be negligible in terms of the ionic balance. This interaction foresees a liquid-solid equilibria, a salt precipitation, which will depend on the solubility product. For example, in case of $CaCl_2$ and NaOH, the solubility products for Eqs. (12), (13) and (14) are 792, 1.3 and 132, respectively. Thus, the ion equilibria, absorption and precipitation processes are affected. Even these ions can interact with the $CaCO_3$ surface, thus influencing the growth habit of the crystals [122,143–145].

According to the experimental setup, operating conditions, absorption and gas mixtures, one of the mechanisms described before, namely absorption, transformation and precipitation, could control the process. Therefore, absorption, chemical reaction and precipitation rates must be considered [150]. Several researchers pointed out that, in the presence of calcium hydroxide or in alkaline solutions, the transformation of aqueous CO_2 into CO_3^{2-} and the precipitation reactions are instantaneous; thus, the CO_2 absorption is the limiting step [119,150,151].

a) Carbonic species and water equilibria

$CO_{2(g)} \rightleftarrows CO_{2(aq)}$	$K_L a$	(2)	
$CO_{2(aq)} + H_2O \rightleftarrows H_2CO_{3(aq)}$	$K_h = 0{,}034$	(3)	
$H_2CO_{3(aq)} \rightleftarrows HCO_{3\,(aq)}^- + H^+_{(aq)}$	$K_{a1} = 4.31 \times 10^{-7}$	(4)	[148]
$HCO_{3\,(aq)}^- \rightleftarrows CO_{3\,(aq)}^{2-} + H^+_{(aq)}$	$K_{a2} = 4.68 \times 10^{-11}$	(5)	[148]
$H_2O \rightleftarrows H^+_{(aq)} + OH^-_{(aq)}$	$K_w = 1 \times 10^{-14}$	(6)	[148]

b) Ion-pair equilibria

$HX_{(aq)} \rightleftarrows H^+_{(aq)} + X^-_{(aq)}$	K_a	(7)	
$BOH_{(aq)} \rightleftarrows B^+_{(aq)} + OH^-_{(aq)}$	K_b	(8)	
$CaHCO_{3\,(aq)}^+ \rightleftarrows Ca^{2+}_{(aq)} + HCO_{3\,(aq)}^-$	$K_{CaHCO_3^+} = 5.50 \times 10^{-2}$	(9)	[148]
$CaOH^+_{(aq)} \rightleftarrows Ca^{2+}_{(aq)} + OH^-_{(aq)}$	$K_{CaOH^+} = 5.02 \times 10^{-2}$	(10)	[148]
$CaCO_3^0 \rightleftarrows Ca^{2+}_{(aq)} + CO_{3\,(aq)}^{2-}$	$K_{CaCO_3^0} = 1.61 \times 10^{-8}$	(11)	[148]

c) Solid-Liquid phase equilibria [152]

$CaX_{2(s)} \rightleftarrows Ca^{2+}{}_{(aq)} + 2X^{-}{}_{(aq)}$	K_{sp1}	(12)	
$BHCO_{3(s)} \rightleftarrows B^{+}{}_{(aq)} + HCO_3^{-}{}_{(aq)}$	K_{sp2}	(13)	
$B_2CO_{3(s)} \rightleftarrows 2B^{+}{}_{(aq)} + CO_3^{2-}{}_{(aq)}$	K_{sp3}	(14)	
$Ca(OH)_{2(s)} \rightleftarrows Ca^{2+}{}_{(aq)} + 2OH^{-}{}_{(aq)}$	$K_{sp-Ca(OH)_2} = 5.5 \times 10^{-6}$	(15)	
$CaCO_{3(s)} \rightleftarrows Ca^{2+}{}_{(aq)} + CO_3^{2-}{}_{(aq)}$	$K_{sp-ACC} = 1 \times 10^{-6}$ $K_{sp-vat} = 1.23 \times 10^{-8}$ $K_{sp-ara} = 4,6 \times 10^{-9}$ $K_{sp-calc} = 3.3 \times 10^{-9}$	(16)	[152]

d) CO_2-alkanolamine aqueous system equilibrium [143]

$CO_{2(aq)} + RNH_2 \rightleftarrows RN^{+}H_2CO_{2(aq)}^{-}$	K_{eq_1}	(17)
$CO_{2(aq)} + R_2NH \rightleftarrows RNHCO_2$	K_{eq_2}	(18)
$RN^{+}H_2CO_{2(aq)}^{-} + RNH_2 \rightleftarrows RNH_{3(aq)}^{+} + RNHCO_{2(aq)}^{-}$	K_{eq_3}	(19)
$R_2NHCO_2 + R_2NH \rightleftarrows R_2NH_{2(aq)}^{+} + R_2NCO_{2(aq)}^{-}$	K_{eq_4}	(20)
$RNHCO_{2(aq)}^{-} + H_2O \rightleftarrows RNH_2 + HCO_{3(aq)}^{-}$	K_{eq_5}	(21)
$R_2NCO_{2(aq)}^{-} + H_2O \rightleftarrows R_2NH + HCO_{3(aq)}^{-}$	K_{eq_6}	(22)

3.2.1. Mass transfer

The mass transfer plays an important role since the creation of supersaturation conditions depends directly on it. Therefore, it has been widely studied by many researchers that stated that the absorption of CO_2 in a suspension of lime is accompanied and boosted by a fast reaction in the gas-liquid film [119,153]. The use of gas mixtures has not a significant effect since the resistance from the gas side can be considered negligible; however, low partial pressures thermodynamically limit the process [119]. The absorption process depends on the inter and intra-molecular phenomena; hence, macro and micromixing influence the absorption performance [150].

In the H_2O-CO_2-Ca^{2+} system, the highest supersaturation levels are reached at the gas-liquid interface because the highest concentration of CO_2 and CO_3^{2-} are present in this region, as can be inferred by considering the film theory of gas-liquid mass transfer followed by chemical reaction. Therefore, the nucleation of $CaCO_3$ takes place near that zone. Then, the precipitated particles diffuse into the liquid bulk where lower supersaturation levels are present and growth is favored. Thus, the mass transfer coefficient has an interesting effect on the $CaCO_3$ precipitation and its properties. For instance, larger mass transfer coefficient values lead to rapid precipitation and smaller particles synthesis [150]. Higher mass transfer leads to lower Damkohler numbers (dimensionless number expressing the reaction rate to mass transfer rate ratio), which indicates that the crystallization process is more homogeneous and higher supersaturation levels can be obtained in the liquid bulk. Consequently, nucleation can be favored over the growth phenomenon. Accordingly, the specific volume of the experimental setup, defined as the ratio between the liquid bulk volume and the gas-liquid surface, V (m^3/m^2), affects the PSD shape, which could be broader or narrower depending on the crystallization mechanism described previously. Hence, for large specific volumes (V>0.002), there are many issues with the control of the PSD as the precipitated crystals at the gas-liquid interface diffuse to the liquid bulk and subsequently, grow. Thus, favoring the synthesis of large particles with a broad PSD as determined by Shun et al. through basic simultaneous equations for the film theory of gas-liquid mass transfer accompanied with chemical reaction coupled to the distributed population and mass balances for crystallization. Otherwise, this drawback can be reduced by employing an experimental setup with a higher specific volume (V<0.002), leading to narrower PSD [150]. Many studies of intensification processes indicate that using a reactor with microchannels with low specific volumes allowed the synthesis of nanoparticles with a narrow PSD [9,45,120,123]. Another way to enhance the mass transfer and reduce the PSD heterogeneity is to implement dispersed CO_2 microbubbles in the liquid, which provides a homogeneous supersaturation and the precipitation in the whole reactor and the gas-liquid surface is higher [47,154].

The mass transfer can also be enhanced by using suitable additives, one of which is terpineol. The polar hydroxyl group (OH) in terpineol is prone to interact with the aqueous phase, while the other nonpolar groups tend to be absorbed on the bubble surface. It is well known that terpineol, which usually exists in the gas-liquid interface, can reduce the surface tension of bubbles, preventing the aggregation of small bubbles and increasing their stability [154]. Even the initial concentration of $Ca(OH)_2$ affects the absorption rate since high concentrations result in a delay in the pH drop due to the continuous dissolution of the $Ca(OH)_2$. Therefore, the CO_2 absorption is fast during the beginning of the carbonation, and the mass transfer coefficient is higher likewise [151]. Nevertheless, the solubility of CO_2 is decreased by the high concentration of electrolytes, i.e. thermodynamically, the process could be affected [151]. The carbonation mechanism affects, consequently, the $CaCO_3$ precipitation mechanism and kinetics.

3.2.2. Precipitation mechanism

In reactive precipitation, chemical reaction, nucleation and growth are the three main steps occurring simultaneously. Therefore, it is worth controlling these three steps during the precipitation. As already stated, high degrees of supersaturation lead to the nucleation of small particles. Then, to obtain $CaCO_3$ nanoparticles, it is important to achieve high supersaturation ratios, uniform spatial concentration distribution and identical growth time for all crystals. Macromixing and micromixing occur simultaneously in the reactors and must be enhanced and homogenized. Uniform spatial concentration distribution of any component on the vessel scale can only be achieved by macromixing, while uniform spatial concentration distribution on the molecular scale can be reached by intense micromixing [155]. Hence, the CO_2 absorption mechanism takes a crucial role in the $CaCO_3$ particles synthesis in order to obtain a high micromixing level. Micromixing is a key factor determining the degree of the supersaturation concentration of the solute and its local spatial distribution [2].

Different precipitation mechanisms can be obtained through the carbonation method, resulting in $CaCO_3$ with numerous morphologies and different sizes and crystal phases. Among the most peculiar morphologies obtained, rhombohedral and spherical particles are the most common [41,48]. Both, the method and the operating parameters can influence the mechanism and habit of the particles, which emphasize the role of the liquid-gas interface on the physicochemical properties of the precipitated particles [156]. Hence, other morphologies, such as hollow particles [58], rhombohedral crystals [49,50], scalenohedral crystals [49], needle-like crystals [32], flower-like particles [87], have been obtained. In addition to the operating parameters, the use of additives can also affect the mechanism of precipitation as described before for the other synthesis methods. In order to control the size, besides to understand and enhance the mass transfer, the kinetics of precipitation, nucleation and growth must be studied.

3.2.3. Carbonation of $Ca(OH)_2$ slurries

The most studied system of carbonation to synthesize $CaCO_3$ particles involves $Ca(OH)_2$ slurries. The carbonation of a $Ca(OH)_2$ slurry at room temperature and without additives generally leads to the synthesis of calcite [8,49,51,55,56,58,62,157–159]. The synthesis from calcium hydroxide is manageable since minor agglomeration issues can turn up. In fact, $Ca(OH)_2$ provide calcite stabilization according to the experimental data published by Kilic et al. [160]. However, size and shape can be tailored by varying the operating parameters of the process. In the carbonation of $Ca(OH)_2$ slurries, the absorption rate mainly influences the $CaCO_3$ crystallization, meaning reactor geometry, CO_2 flow rate, temperature and pH. However, the slurry concentration also influences the process. All these parameters directly affect the Ca^{2+}/CO_3^{2-} ratio (R).

3.2.3.1. Temperature. The influence of temperature is complex because it decreases the CO_2 solubility but affects all the equilibrium constants of the carbonation system. The increase of the temperature entails a higher dissolution of $Ca(OH)_2$ and a lower $CaCO_3$ solubility product (K_{sp}) [16], meaning higher supersaturation ratios and crystallization rates. The agglomeration kinetics is also increased by the temperature [161,162]. Moreover, all these singular processes, nucleation, growth and agglomeration, could be enhanced by increasing the temperature, as this increase could provide the necessary energy for these processes according to the Arrhenius equation [163].

Garcia-Carmona et al. [146] obtained larger crystals by increasing the temperature, meaning that the growth kinetics is more temperature-dependent, indicating it has the highest activation energy. Similar results were obtained by Santos et al., who increased the size of the calcite crystals by increasing the process temperature.

The $CaCO_3$ growth habit can also be controlled by varying the temperature. For instance, Wen et al. [52] obtained plate-like particles at 20 °C, and granular particles at 40 °C. Domingo et al. obtained rhombohedral sharp-edged particles at 45 °C while the presence of scalenohedral particles was observed by decreasing the temperature to 25 °C [49]. Other researchers confirmed these results, reporting agglomerates constituted by small rhombohedral particles obtained at 40 °C and scalenohedral particles at 20 °C, as shown in Fig. 3 [163].

At low temperatures, such as ambient, vaterite formation is possible; however, its conversion to calcite is rapid due to its instability. Carbonation at temperatures above 40 °C makes it possible to obtain a mixture of aragonite and calcite under mechanical stirring without any additive [32]. Santos et al. obtained pure aragonite at temperatures higher than 50 °C and under mechanical stirring [32]. Some studies demonstrated the aragonite formation at high temperatures (>70 °C) starting from $Ca(OH)_2$ slurries [31,32]. Furthermore, in certain cases, depending on the environmental conditions, aragonite transforms to calcite over time due to its metastability [164]. Therefore, the temperature is a favourable factor for the nucleation of aragonite, but not for its stabilization [51,164].

3.2.3.2. $Ca(OH)_2$ slurry concentration. The $Ca(OH)_2$ concentration slurry increases the R-value, which seems to be one of the most important factors influencing the crystallization of $CaCO_3$ in this kind of system. The higher the R values, more boosted is the calcite crystal growth [146,165,166]. This effect is probably due to higher Ca^{2+}/CO_3^{2-} ratios enhancing the formation of a pair of $CaCO_3^0$ growth units at the $CaCO_3$-solution interface. Thus, this favors the calcite growth in the (104) direction [146]. Besides, high R values entail high conductivities, which could have an important effect on the crystal growth, forming scalenohedral crystals, as suggested by Garcia-Carmona et al. [146]. This statement is in good agreement with Gomez-Morales et al. [165], who also indicated that higher $Ca^{2+}/(CO_3^{2-}+HCO_3^-)$ ratios favor the formation of scalenohedral crystals.

Gomez-Morales et al. stated that in the case of an excess of Ca^{2+} ions, the zeta potential (ζ) of calcite crystals is positive, as reported by several researchers [58,160,167,168]. Hence, the HCO_3^- and CO_3^{2-} are easily attached on the crystal surfaced, thus enhancing the crystal growth.

Higher R values also entail higher $CaOH^+$ ion formation, leading to a pH decrease that generates $CaHCO_3^+$ and H^+. These ions interact with negatively charged carbonate ions in the (110) faces, since many carbonates are coplanar with Ca atoms in this direction. This interaction could avoid the growth of the (110) direction and promote this kind of growth [104].

Therefore, the crystal size is highly affected by the $Ca(OH)_2$ concentration. Several researchers reported that higher initial concentrations of $Ca(OH)_2$ normally produce larger $CaCO_3$ particles [158,169,170], since R values are higher and longer synthesis times are needed, thus favoring growth phenomena.

3.2.3.3. Reactor geometry. The range of $Ca(OH)_2$ concentrations influencing the particle dimension varies according to the reactor type and its specific volume (V). Reactors with a specific volume higher than 0.002 m^3/m^2, as stirred reactors, make it possible to synthesize smaller particles but not nanosized crystals when operated at concentrations below 0.1 mol/L. On the other hand, experimental setups with a specific volume lower than 0.002 m^3/m^2, as RPB, and ultrasound-assisted systems favor the synthesis of nanosized crystals when operating with Ca^{2+} concentrations in the range 00.1–0.5 mol/L. Nonetheless, a general trend can be depicted, where higher initial concentrations favor the synthesis of larger crystals. These aspects will be deeply discussed in Section 3.3.

3.2.3.4. CO_2 flow rate. The particle size also increases by decreasing the CO_2 flow rate and its composition in the gas phase since the synthesis times are longer [53,157,170,171]. Furthermore, low CO_2 flowrates decrease the CO_3^{2-} ions production, thus reducing the supersaturation and favouring growth over nucleation. Anyway, these trends can vary from reactor to reactor. For example, conflicting behaviours with respect to the $Ca(OH)_2$ concentration and the CO_2 flowrate were obtained in a bubble column, in a Stirred Tank Reactor (STR) and Couette Taylor (CT), as reported by Wen et al. [52] and Jung et al. [172] respectively. However, the description of these and other experimental setups will be discussed more in detail in Section 3.3.

Similar to the solubility product (K_{sp}) of calcite, which decreases with the temperature, i.e. the solubility is reduced [16], the solubility of CO_2 is reduced as well with the temperature [173,174]. Therefore, the change of the temperature on the carbonation process surely affects the mechanisms and kinetics of both, carbonation and precipitation [49]. Its influence is not clear, but it has been demonstrated that the morphology of calcite is modified.

3.2.3.5. Mixing. The mixing type mainly affects the mass transfer. Both magnetic and mechanical stirring lead to the synthesis of calcite crystals [51,146,175]. In the carbonation of $Ca(OH)_2$ slurreis, the stirring speed does not significantly affect the crystal phase, since generally calcite is

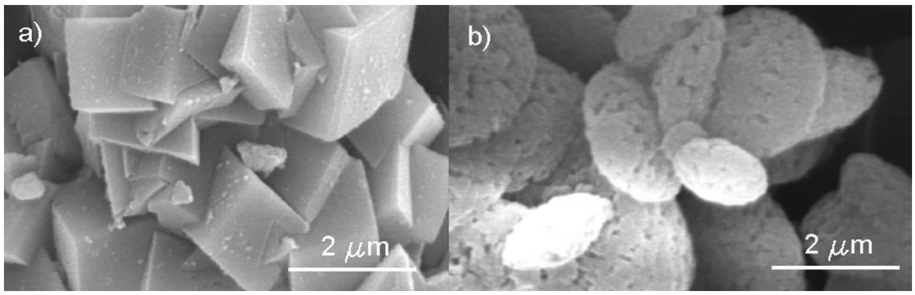

Fig. 3. Effect of temperature on morphology and growth habit of $CaCO_3$. Adapted from [163].

mainly obtained. Nonetheless, the crystal size is reduced by increasing the stirring speed, as the mass transfer is enhanced and the agglomeration is avoided [171,172,175].

The use of ultrasounds instead of mechanical stirring has also been studied [53,169]. It was established that ultrasounds enhance the CO_2 absorption and provide higher supersaturations, which favor the synthesis of smaller particles with a sharper PSD than in the case of mechanical stirring. Furthermore, the use of ultrasounds avoids agglomeration and aggregation phenomena due to the induced cavitation [53,169]. Santos et al. have also suggested that ultrasonic mixing is an additional favourable factor for the nucleation of aragonite [32,176]. They obtained aragonite through carbonation under sonochemical stirring at low temperatures (30–40 °C) without additives. Ultrasound cavitation applies waves in the range of 16–100 kHz, generating high local pressures and temperatures with could promote the nucleation of aragonite [32].

3.2.4. Carbonation of solutions containing $CaCl_2$-CO_2 absorber promoters

Many researchers have been interested in this topic, and the investigations have been carried out through some experimental campaigns [83,163,177]. The interest in this topic comes from the high amount of calcium-rich wastes, which entail a Ca^{2+} solution containing other ions in solution, especially where a CO_2 absorber promoter is involved [125,178]. From these studies, it can be noticed that kinetics is strongly influenced by several factors, such as temperature and presence of ions like NH_4^+, Mg^{2+}, SO_4^{2-} or Cl^-. The presence of these ions could even induce the formation of a preferential crystal phase over the others, as in the case of NH_4^+ or Mg^{2+} that promote vaterite and aragonite, respectively [177]. The effect of temperature, CO_2 flow rate, calcium concentration and other parameters does not have a specific trend. The main remarks of the different systems will be discussed below.

3.2.4.1. $CaCl_2$-NH_4OH-CO_2 system. Several researchers carried out the precipitation of $CaCO_3$ by employing ammonia in order to provide an alkaline medium for CO_2 absorption. They found out that NH_4^+ ions can stabilize vaterite when ammonia is added in excess with respect to calcium and CO_2 (according to Eq. (23)) [11,13,125,136]. This occurs because NH_4^+ ions interact with the CO_3^{2-} ions present on the surface of the negatively charged crystal planes. Here, vaterite presented a spherical morphology, which is its most frequently observed shape [12,136].

$$CO_2 + 2NH_3 + CaCl_2 + H_2O \rightarrow CaCO_3 + 2NH_4Cl \quad (23)$$

$$NH_4OH \rightleftarrows NH_4^+ + OH^- \qquad k_b = 1.78 \times 10^{-5} \quad (24)$$

Spherical calcite particles were obtained by Kim et al. [43] by using $Ca(OH)_2$ instead of $CaCl_2$. This occurs because calcium hydroxide provides high alkalinity, which shifts the equilibrium of ammonium hydroxide (See Eq. (24)) to the left and a lower concentration of NH_4^+ ions is present, disfavoring the stabilization of vaterite. Nevertheless, the presence of NH_4OH modifies the growth mechanism since spherical calcite particles were obtained instead of classical rhombohedral calcite particles [43]. Han et al. controlled and increased the calcite content by decreasing the CO_2 flow rate and concentration [44]. These conditions led to low carbonation rates and longer synthesis times, which induced the vaterite transformation into calcite. Another particular case of production of pure calcite by using gaseous ammonia is reported by Sun et al. [45]. A simultaneous absorption of NH_3 and CO_2 in a $CaCl_2$ solution was performed in a RPB. They obtained pure calcite nanoparticles, probably due to the high gravity effect of the RPB employed, which intensifies the micromixing and therefore the precipitation is intensified too. However, the effect of the RPB will be discussed more in detail in Section 3.3.

3.2.4.2. $CaCl_2$-$NaOH$-CO_2 system. Na^+ ions have a very small ionic radius and they do not have an important role in the crystallization kinetics [179]. The NaOH concentration regulates the pH of the solution, which can influence the $CaCO_3$ polymorphism, and low pH values seem to promote vaterite formation [83]. Chen et al. also demonstrated the effect of the pH. The pH influences the nucleation rate, since the induction time is reduced at pH higher than 10.5–11 [83]. On the other hand, a lower pH leads to higher HCO_3^- concentrations, which favor the formation of $CaCO_3^0$ ion pairs. Thus, the crystal growth was increased under these conditions [41,104,165]. Furthermore, low pH values entail instability leading to a higher formation of HCO_3^- and $CaHCO_3^+$, which interacts with the $CaCO_3$ surface, acting as a link between the precipitated particles to form these nanocrystal agglomerates [58,168].

Marin-Rivera et al. obtained calcite crystals at higher $CaCl_2$ concentrations (20 g/L) [143]. Similar results were obtained by Alamdari et al., who obtained rhombohedral crystals from $CaCl_2$ [177]. This is because the increase of the calcium concentration leads to longer synthesis times, inducing the vaterite transformation into calcite.

Chen and coworkers also individuated the growth dependence on crystal size through seeded tests, from where they concluded that crystal growth of larger particles increased with the crystal size [83]. Hence, it is possible to state that crystal growth mainly depends on temperature, presence of foreign ions, crystal size and supersaturation.

3.2.4.3. $CaCl_2$-$Mg(OH)_2$-CO_2 system. Magnesium ions have been shown to promote nucleation and stabilization of aragonite particles with a high ratio aspect through the carbonation route [6,31,33,35,180]. $MgCl_2$ and $Mg(OH)_2$ are generally used to provide Mg^{2+} ions, which can substitute the Ca^{2+} in calcite to form Mg-calcite because they are very interchangeable [31]. In such a way, the magnesium ions inhibit the calcite growth and favour the aragonite formation [31,180], and by increasing the Mg^{2+} concentration, the content of aragonite increases [35]. Generally, at high temperatures (80 °C), the aspect ratio increases by increasing the Mg/Ca ratio from 3:2 to 5:1 [31,35], but further addition of $MgCl_2$ (Mg/Ca ratio > 5) could favour the formation of pyramidal aragonite particles [31]. Anh et al. suggested that the effect of Mg^{2+} ions also depends on the pH since they observed that the content of aragonite increased by decreasing the pH of the carbonation process by maintaining the same $MgCl_2$ concentration [180].

3.2.4.4. $CaCl_2$-CO_2 system with other CO_2 absorber promoters. Other organic CO_2 absorber promoters, especially amine-based organic solvents, as polyethylenimine (PEI), ethanolamine (MEA), and aminoethylethanolamine (AEEA) have been employed to synthesize $CaCO_3$ crystals through carbonation. The increase in temperature enhanced the absorption-crystallization rate since the decomposition of zwitterion/carbamate is enhanced by increasing the temperature [181]. The temperature increase entails an increment in the crystal size, indicating that the increase in the crystal growth is more temperature-dependent than the other phenomena. A very important aspect to highlight is that mixtures of metastable aragonite and vaterite crystals are obtained by employing these kinds of organic solvents [143]. The gas flow rate did not significantly affect the crystal size, but vaterite crystals were favored over aragonite crystals by increasing the gas flow rate [143].

3.2.5. Calcium-rich wastes carbonation

Several wastes have been employed to synthesize $CaCO_3$ crystals in order to assess the feasibility of the process. Jeon and Kim used seawater and Cement Kiln Dust (CKD) with NaOH in order to basify the calcium solution, and the content of vaterite was modified according to the operating conditions [137]. Low NaOH dosages, i.e. low pH, led to the formation of vaterite. At high CO_2 flow rates, which means higher OH^- ions consumption by the reaction with the

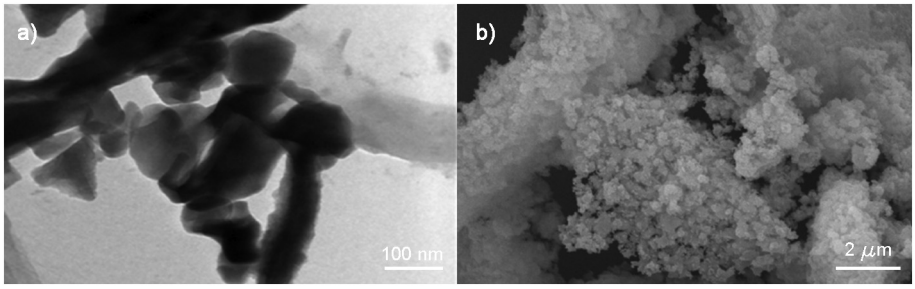

Fig. 4. Representative micrographs of precipitated $CaCO_3$: (a) from pure $CaCl_2$ solution and (b) from distiller waste solution. Adapted from [177].

Table 2
Effect of the impurities present on the distiller waste on the kinetic parameters of the precipitation of $CaCO_3$ through the carbonation route. (CO_2 concentration 20% v/v, 25 °C, 1 atm). Data extracted from experiments published by Alamdari et al. [177].

Calcium solution	Agglomeration constant, k_c ((g solution)$^{-1}$ (μm)^3(s)$^{-1}$)	Nucleation constant. k_n ((g solution)$^{-1}$ (s)$^{-1}$)	Growth constant, k_g (m s^{-1})
Pure $CaCl_2$	1.3×10^{-15}	1415.54	6.08×10^{-10}
Distiller waste	8.80×10^{-13}	894	4.17×10^{-10}

absorbed CO_2, higher contents of vaterite were also obtained [137]. Other researchers have employed CKD to synthesize $CaCO_3$ crystals through the carbonation route [182].

Alamdari et al. studied the mechanisms of nucleation, growth and agglomeration for the precipitation of $CaCO_3$ through CO_2 absorption into a pure $CaCl_2$ solution and into a distiller waste solution from a soda ash plant. In such a way, they determined that the higher ionic strength (by employing the distiller waste solution), i.e. the presence of foreign ions, generates interaction within the $CaCO_3$ clusters, thus reducing the nucleation rate. Foreign ions also interact with the precipitated particles surface, probably by blocking some growing planes, thus influencing the kinetics, but also the mechanism, of growth: in fact, in this case spherical particles with rough surfaces were obtained. On the other hand, rhombohedral particles were synthesized in the case of pure $CaCl_2$, as highlighted in Fig. 4, On the other hand, the agglomeration coefficient was increased, therefore larger particles were synthesized [177]. These results are summarized in Table 2.

Furthermore, they determined that the operating conditions, such as CO_2 concentration in the gas phase or gas flow rate, do not affect the kinetic parameters for nucleation and growth. This is in good agreement with Liu et al., who determined the influence of the temperature [163]. They employed phosphogypsum (PG) as a low-cost calcium resource which was used to prepare $CaCO_3$ crystals. The values of nucleation and growth coefficients increased with the temperature, as summarized in Table 3. Therefore, the temperature influenced even the morphology and habit of particle growth. Small rhombohedral crystals, forming agglomerates and scalenohedral particles, were obtained at 40 and 20 °C, respectively, as illustrated in Fig. 3 [163].

Table 3
Effect of the temperature and CO_2 flowrate on the kinetic parameters of the precipitation of $CaCO_3$ through the carbonation route published by Liu et al. [163].

Temperature	CO_2 flowrate (mL/min)	Nucleation constant. k_n (number/(mol$^{0.8}$m$^{0.6}$min))	Growth constant, k_g (m$^{2.2}$/(mol$^{0.4}$min))
20	138	8.04×10^{16}	2.75×10^{-9}
20	251	9.9×10^{16}	2.73×10^{-9}
30	138	9.73×10^{16}	4.13×10^{-9}
30	251	1.73×10^{17}	4.27×10^{-9}
40	138	1.21×10^{17}	9.81×10^{-9}
40	251	1.51×10^{17}	9.36×10^{-9}

The effluent from the soda ash manufacturing process (Solvay) has also been employed to prepare $CaCO_3$ crystals [81,135,140,178]. Somani et al. emulated the Solvay waste and obtained different $CaCO_3$ polymorphs according to the employed calcium concentration. They observed that calcite crystals were favored at concentrations higher than 1 mol/L, while a small amount of aragonite crystals were present at lower concentrations [81].

Czaplicka and Konopacka-Łyskawa also emulated the Solvay effluent using ammonia as the CO_2 absorption promoter [178]. They obtained mainly vaterite crystals regardless of the concentration of the reactants with sizes below 5 μm, employing a gas flow rate equal to 30 dm^3/h [178]. Czaplicka et al. employed other kinds of CO_2 absorption promoters, such as triethanolamine (TEA) and triethylamine (Et_3N), to evaluate their effect on the process. They obtained mainly vaterite when TEA was employed as CO_2 absorption promoter, and mainly calcite crystals when Et_3N and NH_4OH were employed [140]. These results differ from their previous study because they employed a higher gas flow rate in this study (60–80 dm^3/h). According to the SEM micrographs, the smallest crystals were obtained using Et_3N with sub-micrometric size but high degree of agglomeration. In fact, the PSD showed a bimodal distribution with a sub-micron population and another one around 5 μm. The use of Et_3N also led to the synthesis of sharp-edged crystals, while with NH_4OH and TEA, crystals with a higher rough surface and larger sizes were observed [140].

3.3. Reactors

Several reactors and experimental setups have been employed to synthesize $CaCO_3$ nanoparticles. They are illustrated in Fig. 5 and are summarized in Table 4 with detailed information about their performance, mainly expressed in terms of reagents employed, obtained polymorphism, particle size and CO_2 conversion.

In a gas stirred tank reactor (STR), various types of mixers and sparger design can be used to create homogenous mixture of both calcium hydroxide suspension, $CaCO_3$ particles suspension and gas bubbles created in the reaction system. The gas phase can be fed to the reaction mixture by a surface contact, nozzles in the bottom part of the vertical baffle or sintered glass [183]. The performance of a gas-sparged STR is strongly linked to the sparger design [184]. Tank contactors with flat-blade turbine stirrers were used by Kakaraniya et al. [185] and Ukrainczyk et al. [186]. They obtained microparticles with dimensions of 4 μm and 0.02–2 μm respectively, whereas uniform calcite nanoparticles with the mean size of 24–110 nm nanoparticles were synthesized by means of a surface-aerated tank reactor [185,186]. Several morphologies were obtained by varying the sparger design, such as hollow and rice-like particles [58,62,175]. The sparger design directly affects the K_La; thus, influencing the whole precipitation mechanism while the stirring velocity influences the gas-liquid interface. Traditional STR provide low mass transfer coefficients around 10^{-3} 1/s according to numerical correlations extracted from

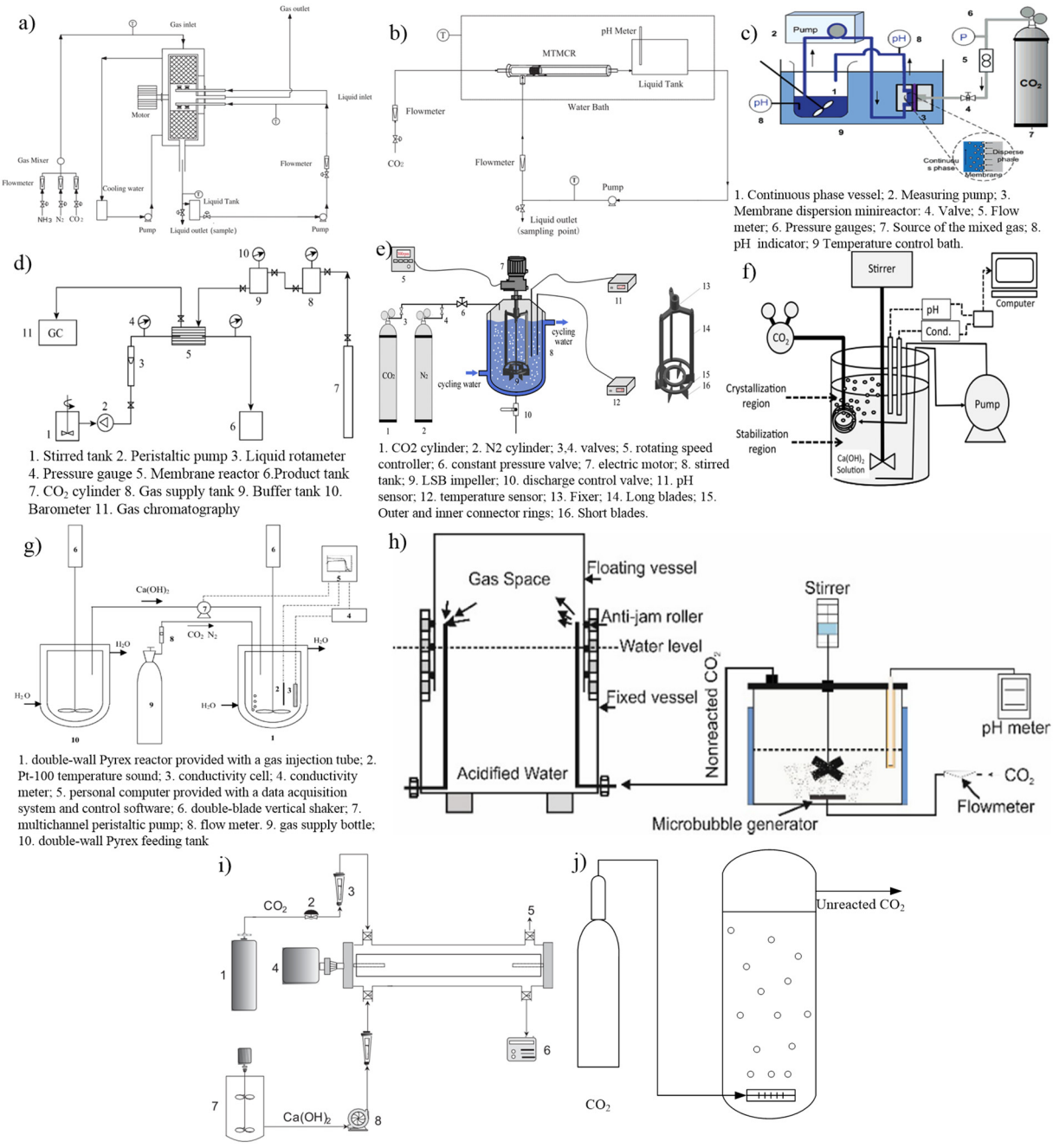

Fig. 5. Different experimental setups-reactors employed for the synthesis of $CaCO_3$ through carbonation route. a) Rotating Packed Bed reactor; b) Microporous tube in tube microchannel reactor; c) Microstructure minireactor; d) G-L Membrane Contactor; e) Surface-aerated stirred tank; f) Jet flow reactor; g) Gas sparged stirred tank reactor; h) Microbubble generator; i) Couette Taylor reactor; j) Bubble column.

the literature [187,188] and results obtained experimentally [184,187,189–192].

Liendo et al. obtained calcite microparticles with broad PSD in a magnetic STR starting from a $Ca(OH)_2$ slurry [175]. Slightly smaller calcite crystals were obtained by Jung et al. by employing a mechanical STR [172]. Several researchers have employed mechanical STR, and most of them obtained dispersed calcite crystals with sizes larger than 200–300 nm [169] [47,62]. The morphology of the calcite crystals obtained with these kinds of reactors was scalenohedral forming laminated crystals [47,146,175].

Another strategy to enhance the process is by modifying the bubbling method. Atliner et al. employed a microbubble generator (MBG), in which the small size of the generated bubbles provides a considerably higher mass transfer surface than those of conventional bubble STR. Thus, favoring the formation of smaller particles and higher CO_2 conversions [47,193]. Ulkeryildiz et al. fed the CO_2 through an orifice in the proximity of the liquid surface in order to allow the undissolved CO_2 to be purged into the atmosphere. In the vicinity of the orifice, the $CaCO_3$ crystallizes and, by the action of the mechanical stirring, the crystals are pumped into the bulk, and new $Ca(OH)_2$ arrive to react with the CO_2 [62]. They also used a jet flow reactor in another work [58]. This consisted in a mechanically stirred reactor with the liquid recirculation in a portion of volume close to a coil pipe with holes from where the CO_2 is fed. In such a way, the contact between gas and liquid occurs and the $CaCO_3$ particles are formed; subsequently, the pumped liquid drives them into a $Ca(OH)_2$ rich zone to stabilize them

Table 4
Carbonation-precipitation performance of different reactors. Polymorphism, Particle size and CO_2 conversion.

Reactor	Reagents	Polymorphism	Particle size (d_p, nm)	CO_2 conversion	Ref.
Rotating packed bed (RPB)	$CaCl_2/NH_3/CO_2$ $Ca(OH)_2/CO_2$	Rhombohedral calcite	44–72 17–36	Not reported	[45,170]
Microporous tube in tube microchannel reactor (MTMCR)	$Ca(OH)_2/CO_2$	Rhombohedral calcite	25–70	6-52%	[123]
Microstructure minireactor (MSMR)	$Ca(OH)_2/CO_2$ (29.8% v/v)	Rhombohedral calcite	39–110	20%	[199]
G-L Membrane Contactor (MC)	$Ca(OH)_2/CO_2$	Rhombohedral calcite	75–80	Not reported	[46]
Surface-aerated stirred tank (SASR)	$Ca(OH)_2/CO_2$	Rhombohedral calcite	24–110	>95%	[171]
Gas sparged stirred tank reactor (STR)	$Ca(OH)_2/CO_2$	Spherical [47], hollow [58], rice-like [62] and rhombohedral [146] calcite	100–2000 [47] 400 [58] 900 [62] >6120 [146]	1-21% [47] 50% [58] 11% [62] <9% [146]	[47,58,62,146]
Microbubble generator (MBG)	$Ca(OH)_2/CO_2$	Rhombohedral calcite	80–530	2-27%	[47,193]
Couette Taylor (CT)	$Ca(OH)_2/CO_2$	Rhombohedral calcite	5–12	Not reported	[172]
Closed loop Reactor (CLR)	$Ca(OH)_2/CO_2$	Rhombohedral calcite	50–100	16 %	[48]
Bubble column (BC)	$Ca(OH)_2/CO_2$	Plate like and spherical calcite	100–1750	4–8%	[52]

[58,160]. The coil pipe is placed in the upper corner, so crystallization and stabilization zones are created. This setup promoted the production of submicron particles and CO_2 conversions were equal to 50%, higher than that obtained in other STR setups.

STR reactors show poor mass transfer coefficients (low Da numbers), meaning slow rates of carbonation and formation of CO_3^{2-} ions, which is rapidly consumed by the reaction with the Ca^{2+} ions [151]. In these cases, the process is controlled by the absorption of CO_2 [151]. Under such conditions, the supersaturation ratio is low. Hence, the growth is promoted, and it's unlikely to obtain small particles such as nanoparticles.

The segregation issues often observed in conventional mechanically-STRs generally led to the synthesis of large particles with wide PSD [45,47]. An increase in the initial calcium concentration can be performed to overcome this issue. This leads to an increase in the initial supersaturation and a reduction of the induction time. As a result, smaller particles can be synthesized [125,165,194].

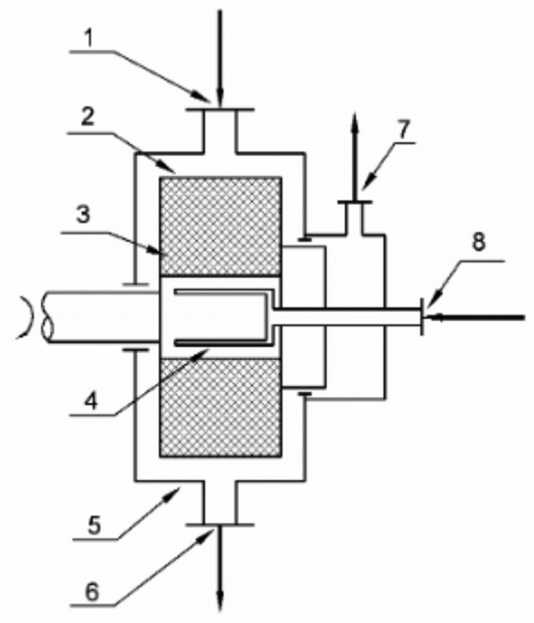

Fig. 6. Countercurrent RPB structure. (1) gas inlet; (2) rotator; (3) packing; (4) Liquid distributor; (5) casing; (6) liquid outlet; (7) gas outlet; (8) liquid inlet. Extracted from reference [217]. This figure was published in China Particuology, Vol 1, Jianfeng Chen and Lei Shao, Mass production of nanoparticles by high gravity reactive precipitation technology with low cost, Page 64-69, Copyright Elsevier (2003).

Couette Taylor reactor, surface-aerated stirred tank and closed-loop reactor are among other experimental setups that have been employed to synthesize $CaCO_3$ crystals through carbonation. These setups exploit the bubbling in a liquid bulk to absorb CO_2 and can reduce the segregation issues. In a Couette Taylor (CT) reactor, calcite micrometric particles were obtained [172]. The CT, unlike STR, provides homogeneous crystals since the unique mixing behavior of the Taylor vortices effectively encouraged homogeneous mixing conditions [172]. The surface-aerated stirred tank (SASR) provides appropriate conditions to synthesize nanoparticles and CO_2 conversions higher than 95%. In such a setup, the CO_2 is continuously fed during the whole process to make up the CO_2 consumed by the reactions in the liquid to keep a constant pressure of 400 kPa, making possible to obtain these high CO_2 conversions [171]. The closed-loop reactor (CLR) also led to the production of nanoparticles, as reported by Thriveni et al., with CO_2 conversions equal to 16% [48]. Bubble columns (BC) gave the possibility to obtain plate-like microparticles or spherical nanoparticles as the initial concentration of calcium increased [52].

Segregation issues can also be reduced and avoided by process intensification [120]. Process intensification is widely exploited in the absorption and precipitation process [123,176,195]. High-gravity and sonochemical processes enhance both absorption and precipitation since the turbulence and micromixing are improved. An improved micromixing leads to the synthesis small particles with a narrow PSD [9,45,53,170,196].

For instance, by employing sonochemical STR an enhanced mass transfer and reduced Da number can be achieved with low calcium concentrations [169]. In fact, the use of ultrasounds induces cavitation with high-frequency mechanical waves, and this phenomenon affects the reaction system. Upon fragmentation of the bubble, the radicals generated therein get released into the medium, where they can induce or accelerate chemical reactions. Therefore, an enhanced mass transfer with a homogeneous mixture is provided, and agglomeration is additionally avoided. Furthermore, ultrasounds generate radical interaction with cations, thus enhancing the precipitation kinetics to obtain a product with higher crystallinity and sharp size distributions.

A Packed Bed Reactor was employed by Liendo et al. to produce nanosized rhombohedral calcite crystals [175]. They attributed the reduction in size with respect to the results obtained in a STR to the increased mass transfer that this kind of reactor can provide (around 10^{-2} 1/s) [175]. Furthermore, the turbulence in the PBR enhanced the micromixing and allowed the synthesis of nanosized crystals. They concluded that the flow regime strongly influences the $CaCO_3$ crystallization through carbonation.

Another experimental setup that exploits improved gas-liquid mass transfer and micromixing is the RPB, which is a high-gravity device that

Table 5
Main effects of additives on properties of $CaCO_3$ particles via carbonation precipitation.

Additive	Additive type	Concentration	Operating conditions	Main effect	Application(s)	Ref.
NH_4^+	Ion	NH_4^+/Ca^{2+} ratio > 1	Low pH	Promote vaterite formation	Some of vaterite applications	[43,125,136]
Mg^{2+}	Ion	Mg^{2+}/Ca^{2+} ratio > 1	Low pH Temperature >30 °C	Promote aragonite formation	Some of aragonite applications	[31,180]
$Eu(NO_3)_3$	Inorganic additive	0.01–0.08 mol/L	T = 0–15 °C	Reduced the particle size of rhombohedral crystals	Optical materials	[158]
			T = 25–45 °C	Favored the formation of spindle like crystals		
Phosphoric acid	Inorganic additive	3.5–10 g/L	70 °C	Promoted aragonite formation	Filler in plastic, rubber and paper industry	[9]
PAA	Organic additive	0.75 g/L	95 °C	Promoted aragonite formation	Pulp and paper industry	[164]
Sucrose and glucose	Organic additive		In the presence of Mg^{2+} ions	Promoted calcite over aragonite	Some of calcite applications	[31]
Terpineol	Monoterpene alcohol	0.1–1%	Room conditions. CO_2 25% v/v	Smaller CO_2 bubbles and decreased d_p.	Polymer filler	[154]
Ethanol	Alcohol	10–50% v/v	NH_4^+/Ca^{2+} ratio = 1	Favored vaterite over calcite	Some of vaterite applications	[136]
			NH_4^+/Ca^{2+} ratio > 1	Favored aragonite over vaterite	Some of aragonite applications	
PAM	Anionic Polyacrilamide	0.02%	T = 20 °C	Increased the $CaCO_3$ by controlling aggregation and enhanced carbonation	Not reported	[205]
			T = 40 °C	Promoted aragonite formation	Plastic and paper filler	
EDTA	Chelating agent	0–0.003 mol/L	Room conditions. CO_2 25% v/v	Promoted the synthesis of $CaCO_3$ nanoparticles (Size < 100 nm)	Filler of plastics, rubber and paper	[206]
Oleic acid	Surfactant	0–3.5% wt	5 °C < T < 25 °C In the presence of ethanol	Reduced the $CaCO_3$ size	Material reinforcement	[207]
CTAB	Cationic surfactant	2%	80–530	Reduced the d_p and favoured rhombohedral shape	Paper coating	[209,210]
SDS	Anionic surfactant	2 g/L	Room temperature and 4.9–12.04 MPa	Favours hombohedralcalcite particles with rough surface	Not reported	[211]
Tween 80	Non ionic surfactant	2 g/L	Room temperature and 4.9–12.04 MPa	Promotes aggregated plate like nano particles	Not reported	[211]
ODHP		0–2%	Room conditions. CO_2/N_2 mixture	Reduced particle size. Provided hydrophobicity to $CaCO_3$	Filler in plastics, rubber and paint	[212]
PGP	Polymer	0.2–0.4%	Room conditions. CO_2 33% v/v	Modified the $CaCO_3$ Chain like particles were obtained by increasing the PGP concentration	Increasing the in-situ polymerization degree and thermal stability of PET	[213]
PGP-NaOH-SA mixture	Polymer	2%	Room conditions. CO_2 33% v/v	Surface modification. Hydrophobic particles.	Filler of PET	[214]
Petroleum sulfonic acid	Oil dispersion	Not specified	Oil dispersion (heptane, etOH and NH_3)	d_p about 10-30 nm with narrow PSD	$CaCO_3$ based nanodetergents as lubricants	[215]
HABS	Oil dispersion	Not specified	Oil dispersion (MetOH and diluent oil)	d_p about 10-30 nm	$CaCO_3$ based nanodetergents as lubricants	[216]

provides a kLa equal to 10^{-1} 1/s [197]. The RPB setup is illustrated in Fig. 6. The gas is fed from the outer edge to the inner edge of the rotor, while the liquid is fed in the edge of the rotor and flows through the rotating packing to the outer edge by the action of centrifugal force. The gas stream comes in contact with the liquid one in the packing bodies in counter-current mode. In there, CO_2 is absorbed by the liquid and reacts to form $CaCO_3$. The liquid, flowing through the packing, forms a thin film under the high shear field. Due to the very high turbulence and dispersion, the large interface renewal rate and the thin films (10–80 μm) of liquid in the RPB, the mass transfer of CO_2 is greatly enhanced, resulting in a great increase in the nucleation rate [45]. Micromixing (i.e., mixing at the molecular scale) is the last stage of turbulent mixing and consists of the viscous-convective deformation of fluid elements, followed by molecular diffusion [120]. Nucleation time is strongly dependent on induction time (τ). From the viewpoint of chemical reaction engineering, the reaction rate and subsequent nucleation in precipitation is controlled by the intrinsic kinetics without the influence of micromixing in the region of $t_m < \tau$ and controlled or influenced by micromixing when $t_m > \tau$. In the RPB, the t_m is about 0.1 ms and smaller than τ (1 ms) [170,198]. RPB has lower t_m than several reactors, such as STR, CT, US-assisted reactors, CLR, etc. [45]. Therefore, RPB reactors have been successfully employed for the synthesis of nanoparticles with very sharp PSD.

Rhombohedral calcite nanoparticles were obtained by employing both $CaCl_2$ and $Ca(OH)_2$ in an RPB, although calcium hydroxide led to the synthesis of smaller crystals and narrower PSDs [45,170]. Wang et al. synthesized $CaCO_3$ in a RPB and the CO_2 flowrate was determinant on the crystal phase, morphology and size. Higher CO_2 flowrates enhanced the carbonation rate, hence the CO_3^{2-} ion concentration and thus the supersaturation increased, leading to a higher calcite content with a lower content of short needle-like particles due to shorter synthesis times as well as growth times. On the other hand, small flowrates then led to higher aragonite content and higher aspect ratio [9]. These results are in good agreement with experimental data published by Altiner and Yildirim [33] and Santos et al. [32]. The rotating speed had also an important role. By increasing the rotating speed of the RPB from 600 to 1200 rpm, the aragonite content and particle length were increased, while the particle diameter was reduced, therefore the aspect ratio was higher. A further increase of the rotating speed led to calcite formation, probably due to the enhancement of carbonation, thus producing a higher supersaturation, which favours the calcite formation as in the case of high CO_2 flowrates [9].

The Microporous tube-in-tube microchannel reactor (MTMCR) represents another intensification alternative that favored the formation of nano calcite starting from $Ca(OH)_2$ with a CO_2 conversion up to 52% at low CO_2 flow rates [123]. Rhombohedral calcite nanoparticles were obtained in a microstructure mini-reactor (MSMR) starting from $Ca(OH)_2$ and employing diluted CO_2, which was converted by 20% [199]. In a membrane contactor (MC), also nano calcite was obtained [46].

In the RPB, as well as other reactors as MTMCR, and MSMR, where the liquid is continuously recirculated (as illustrated in Fig. 5a,b,c, and k), the effect of the liquid is also important, and hence it has been determined. Sun et al. determined that an increase of the liquid volumetric flow rate generated an increase of the gas-liquid interfacial area and mass transfer, which increased $CaCO_3$ nucleation rate and decreased the mean particle size of $CaCO_3$ [45]. By employing CLR, MTMCR, and MSMR, the trend of the effect of the liquid flow rate was very similar to that observed by Sun et al. [48,123,199].

On the other hand, ultrasounds-assisted carbonation, RPB, MTMCR, and MSMR, are setups that enhance the carbonation process, i.e., lower Da numbers. In these cases, the process is controlled by intrinsic kinetics, hence provides high supersaturation rapidly, which favors the rapid formation of small particles that subsequently grow. By increasing the initial concentration of $Ca(OH)_2$, the synthesis time would be increased under Ca^{2+}/CO_3^{2-} ratio and supersaturation conditions favoring growth over nucleation [146].

Similar contradictions can be found among the results of some works concerning the effect of the gas flow rate. Sun et al. observed that the particle size decreased by increasing the gas flow rate in an RPB and attributed this trend to the reduction of the synthesis time [45], in good agreement with other research works carried out with different experimental setups [123,199]. Instead, MBG showed an opposite trend according to the data from the experiments of Altiner et al. [47]. This reactor favored the formation of very well dispersed small bubbles, avoiding the segregation issues normally present in the traditional STR [45,47]. These advantages were reduced by increasing the gas flow rate, favoring larger particle synthesis [47,193]. Again, the Da number influences the performance of the experimental setup. Low Da numbers lead to the synthesis of small particles. Therefore, if the increase of the gas flow rate decreases the Da number of the experimental setup, as in the case of the RPB or STR, the particle size will be decreased. Otherwise, the synthesis of smaller particles will be favored by decreasing the gas flow rate, as in the case of the MBG.

3.4. Additives

Additives are very useful to obtain $CaCO_3$ particles with a specific polymorphism. While calcite particles can be produced without additives, they are largely employed to synthesize vaterite and aragonite particles. Nevertheless, even for calcite particles, some additives are employed to control the size or morphology. Table 5 summarizes the main effects of additives on the $CaCO_3$ properties obtained via the carbonation-precipitation route.

Ammonium ion-based compounds are widely used as additives to promote the synthesis of vaterite particles. Under stoichiometric conditions ($NH_3/Ca^{2+} = 2$), calcite is the predominant phase present in the mixture [43,125,136], while pure vaterite particles can be obtained under excess of ammonia [136]. Song et al. increased the content of spherical vaterite particles under stoichiometric conditions by adding ethanol, but under ammonia excess conditions and in the presence of ethanol, aragonite formation was observed [136].

Other inorganic additives have been employed to tune the $CaCO_3$ properties. Rhombohedral and spindle-shaped $CaCO_3$ particles doped with Eu^{3+} ions, with potential applications as optical materials with strong red emission, were synthesized by the addition of $Eu(NO_3)_3$ [158]. The europium nitrate reduced the particle size of the rhombohedral particles (CaO concentration 0.5–1 mol/L) but did not affect the spindle-shaped particles (CaO concentration 1.5–4 mol/L). According to XRD analysis, Zhou et al. stated that only calcite was detected, indicating that Eu^{3+} ions have successfully entered into the $CaCO_3$ host lattices [158]. According to their analysis, the spindle-shaped $CaCO_3$:Eu^{3+} showed a far weaker luminescence than rhombohedral $CaCO_3$:Eu^{3+} under the same measurement conditions, attributed to the different internal and surface defects of the matrix [158].

Mg^{2+} ion is the most effective ion additive to promote aragonite synthesis. However, its effect depends not only on its concentration but also on other factors like Ca/Mg ratio, temperature, pH, and presence of other additives, as mentioned before [31,180].

Phosphoric acid has also been tested as aragonite promoters without the use of magnesium [9]. The H_3PO_4 content controls the morphology in a carbonation synthesis carried out at 70 °C in a Rotating Packed Bed (RPB) reactor, passing from spindle calcite particles without additive to needle-like aragonite crystals with a concentration of 7 g/L. The aspect ratio increased with the H_3PO_4 content, although the diameter of the needle-like particles (500 nm) remained constant. A further increase of the H_3PO_4 content did not change the phase control [9]. Phosphoric acid reacts with $Ca(OH)_2$ before the carbonation process, thus producing very fine and needle-like hydroxyapatite particles [200,201], which act as heterogeneous nucleators, and the aragonite growth takes place on them [9].

Polyacrylic Acid (PAA) has also been tested as aragonite promoters and seems to stabilize the aragonite phase. It is because the polyacrylate ions can react with the Ca^{2+} ions to form a complex on the surface in the c-axial direction of the needle-like aragonite crystal [164]. This compound causes a delay of the crystal growth in the direction perpendicular to the c-axis and thus the stabilization of aragonite crystals. Hence, it influences the formation and growth of aragonite whiskers, while the calcite formation is restrained [164]. Therefore, Pan et al. obtained stable aragonite particles at high temperatures (>40 °C) through the carbonation route [164].

Other organic additives, such as glucose, sucrose, citric acid, malic acid and phthalic acid have been tested with magnesium chloride in order to determine their effect on the formation of aragonite through the carbonation route [31]. Glucose and sucrose inhibit the formation of aragonite, even in the presence of $MgCl_2$ [31]. Phthalic acid does not influence the formation of aragonite, but promoted the crystal face (2 2 1) of the aragonite [31]. Therefore, the effect of the additives on the aragonite formation depends on their structural characteristics. For instance, glucose, sucrose, citric acid and malic acid may disrupt the aragonite formation by reacting with magnesium ions, thus reducing its effect of aragonite promotion. On the other hand, phthalic acid chelates to calcium ions with its two carboxylic groups and this chelation may be associated with the specific crystal face and the yield of aragonite [31].

Terpineol, monoterpene alcohol, has also been employed to synthesize $CaCO_3$ particles by Xiang et al. [154]. Terpineol enhances the absorption of CO_2 and leads to smaller particles. By increasing the terpineol content from 0.1% to 1%, it was possible to decrease the particle size [154]. Besides, Terpineol increases the stability of small CO_2 bubbles and prevents their coalescence, enhancing the mass transfer of CO_2 into the solution and favoring the formation of $CaCO_3$ fine particles [154]. Nevertheless, further addition of terpineol (>1%) led to the synthesis of larger particles with an irregular shape [154]. This terpineol effect was not noticed when employed in an experimental setup with poor mass transfer coefficients like that used by Feng et al. [157].

Alcohols have also been employed as additives to stabilize vaterite crystals [136,202,203]. Some experiments with a certain ethanol content led to the synthesis of vaterite crystals in the presence of stoichiometric amounts of ammonia and calcium. This is because ethanol interacts with the Ca^{2+} ions, thus forming "solvent cages" to shield Ca^{2+} on CO_3^{2-}, which can reduce the activity of CO_3^{2-} during the reaction [204]. Nevertheless, in the case of ammonia excess, a high ethanol content could favor the formation of aragonite [136]. On the other hand, glycine negative ions migrates to Ca^{2+}, thus participating in the nucleation of $CaCO_3$ and stabilizing the primary vaterite particles [202,203]. Moreover, Guan et al. pointed out that there is a co-effect of glycine molecular and gas-liquid interface, i.e. the bubble method influenced also the polymorphism of particles [203].

Polyacrylamides (PAMs) have been used to control the morphology and particle size during the carbonation process. During PCC synthesis, the use of anionic PAM promoted the aggregation of unreacted calcium hydroxide particles and calcium carbonate nuclei, leading to an increase in aggregate size and reduced reaction time for the carbonation process [205].

EDTA has been used to control the $CaCO_3$ particle size. The presence of EDTA accelerated the carbonation rate. A faster carbonation process was favorable to nuclei formation and led to the formation of superfine particles with a diameter of less than 100 nm [206]. Also, surfactant additives have been employed to control particle size. Monodispersed $CaCO_3$ nanoparticles have been synthesized by introducing CO_2 through a tube into a $Ca(OH)_2$ slurry added with an ethanol solution of oleic acid. A proper amount of oleic acid prevents the growth of the nanoparticles through the deposition of resultant from oleic acid and Ca^{2+} as hydrophobic $Ca(C_{17}H_{33}COO)_2$ on the surface of $CaCO_3$ nanoparticles [207]. However, when the amount of oleic acid is excessive, although the growth is restrained, the particles tend to agglomerate due to the carbon-carbon double bond attached to the surface of $CaCO_3$ crystals, as stated by Wang et al. [207,208].

Additionally, the surfactant influenced the PCC structural properties, such as the pore size distribution and the surface area [209,210]. The addition of CTAB (hexadecyltetramethylammonium bromide) or sodium oleate additives (up to 2 wt%) inhibited particle growth and led to rhombohedral particles of 20−100 nm rather than microsized scalenohedral particles. CTAB- and oleate-modified calcium carbonate nanoparticles are heavily useful in paper coating because they improve paper properties such as smoothness, brightness, whiteness, and opacity [209]. Zhang et al. also employed CTAB, but they did not find any significant effect on the morphology and size by its employment [211]. However, other surfactants as sodium dodecyl sulphate (SDS) and polyoxyethylene-80-sorbitan monooleate (Tween 80) were employed by Zhang et al. [211]. They stated that, in the presence of SDS, alkyl chains carry negative charges, which can be absorbed onto the positively charged faces of $CaCO_3$, inhibiting their further growth and leading to the formation of rhombohedral particles with a rough surface.

On the other hand, Tween 80 is a kind of non-ionic surfactant. It was preferably absorbed on the neutral faces of the $CaCO_3$ crystal leading to the formation aggregated plate-like crystals along the c-axis. The increment of the pressure led to larger particles (2–4 μm) [211].

Moreover, octadecyl dihydrogen phosphate (ODHP) was added as an additive, acting on the crystal growth and controlling the $CaCO_3$ size [212]. The additive concentration was varied from 0 to 2%, being 1% the optimal dosage for the crystal size since smaller particles were obtained. This additive modified the surface of the PCC. It seems to react with bicarbonate and calcium ions, thus modifying the $CaCO_3$ surface and making it possible to obtain hydrophobic $CaCO_3$ particles. Therefore, superfine calcite particles were obtained by Sheng et al. by employing octadecyl dihydrogen as an additive [212]. Thus, this surface modification of calcium carbonate with hydrophobic species would lead to a great expansion of applications of $CaCO_3$ as filler in plastics, rubber, and paint, since mineral particles are hardly dispersed in a polymer matrix [212].

Furthermore, polyethylene glycol phosphate (PGP) has been employed as an additive modifying the $CaCO_3$ surface. In the experiments performed by Chen et al., calcite grew in the classical rhombohedral shape with a particle size between 40 and 60 nm in the absence of PGP. Similar particles (40 nm) but with high roughness were obtained with 0.2% of PGP, which indicates its deposition on the $CaCO_3$ surface. Instead, with 0.4%, the morphology changed considerably, and chain-like aggregated nanoparticles with size from 50 to 500 nm were obtained [213]. The results proved that the PGP/$CaCO_3$ weight ratio could be considered an alternative and versatile tool for adjusting the morphology and the size of the crystals. At the beginning of the crystallization process, the nucleated $CaCO_3$ adsorbs PGP due to the electrostatic potential interactions between PGP and Ca^{2+}. Thus, the adsorption of organic matter on calcite can balance the relative loss in the crystallization energy and promote the nucleation of primary calcite nanoparticles coated by PGP. At a low PGP/$CaCO_3$ ratio, most PGP molecules exist in the form of micelles, and the number of free PGP molecules is few. So, the effect of PGP on morphology is not obvious. As PGP/$CaCO_3$ ratio increases, the number of the free PGP molecules increases, so the formation of chain-like nanoparticles is favored. The formation of such structures is due to the primary $CaCO_3$ nanoparticles adsorbed by PGP which preferentially interact with the head group and oxygen atoms of the free PGP via hydrogen bonds, causing small entities aggregation to occur and yielding to well-oriented polycrystalline aggregates. The crystals develop along the PGP chain until they collide with each other [213]. These particles were employed for the in-situ preparation of poly (ethylene terephthalate) (PET), and the resulting nanocomposite filled with the modified $CaCO_3$ exhibited a better dispersion of the nanoparticles, a higher polymerization degree, and better thermal stability [213]. Furthermore, PGP deposition on $CaCO_3$ inhibits the reaction between $CaCO_3$ and TPA, leading to some difficulties in the in-situ preparation of $CaCO_3$/PET. Therefore, these nanocomposites avoid the high costs required for the fabrication of conventional PET [213].

Chen et al. [214] also used PGP mixed with NaOH and stearic acid (SA) as an additive. This method effectively made it possible to produce hydrophobic $CaCO_3$ during the carbonation at room temperature, unlike results with only PGP [213]. SA increased the hydrophobicity of $CaCO_3$, and a 2% addition favored the synthesis of completely hydrophobic $CaCO_3$ particles [214]. Also, NaOH showed an interesting effect on the hydrophobicity of the $CaCO_3$: its presence provided hydrophobicity to $CaCO_3$. Nevertheless, it showed a maximum at 0.5% due to the electrostatic interaction with SA, which could inhibit the $CaCO_3$ surface modification by SA. PGP notably increased the hydrophobicity of the $CaCO_3$ particles and remarkably modified the morphology since the aggregation increased with the PGP concentration. This increase led to a lower available surface of $CaCO_3$, and the SA could modify the entire $CaCO_3$ surface. In this work, the researchers also made some considerations regarding the mechanism of formation of $CaCO_3$ with these additives and divided the process in two main steps, nucleation of $CaCO_3$ and their aggregation. At the beginning of the nucleation process, SA and PGP generate a certain preferential orientation at the $Ca(OH)_2$–$CaCO_3$–CO_2 interface [214]. Due to the electrostatic potential interactions between SA and Ca^{2+}, SA is adsorbed on $CaCO_3$ while soluble PGP exists at the interface in the form of the micelles and free PGP molecules [214]. The micelle can play an important role in increasing SA, and free PGP molecules solubility could play a function as a template in the crystallization process [214]. Calcium ions absorbed by SA interact with the head group and oxygen atoms of PGP via the covalent bond and hydrogen bonds, respectively [214]. A high ratio of PGP/$CaCO_3$ allows the nucleation of particles over the PGP chain until they collide with each other. Instead, at low ratios, short chains of rhombohedral particles are obtained in agreement with their previous results about the influence of PGP [213]. These hydrophobic particles were considered to be tested for the in-situ preparation of PET.

Oil dispersion of $CaCO_3$ to be employed as nano detergents has also been synthesized through the carbonation route using additives [215]. Kang et al. used petroleum sulfonic acid (Ar-SO_3H (Ar-:aryl group), purity N66 wt%, inorganic acid b3 wt%, Mn ≈ 470), ethanol, heptane, and ammonia [215]. Besides, they employed an RPB to overcome different carbonation challenges in STR that make them inefficient [215]. They obtained more monodispersed particles by employing the RPB. The as-prepared liquid-state nano-detergents were constituted of $CaCO_3$ nanoparticles coated with an oil-soluble surfactant of [$Ca(Ar\text{-}SO_3)_2$] monodispersed in oil, which showed an average particle size of 6 nm, high stability of >18 months, and solid content of 38.5 wt%. This product should have a good performance as a lubricant for modern machines [215]. $CaCO_3$-based nano-detergents were also prepared by carbonation using heavy alkyl benzene sulfonate acid (HABS), methanol and diluent oil [216]. The formation of $CaCO_3$ calcite from ACC via vaterite was identified through XRD analysis. The effect of the methanol

content, CaO/total alkalinity calcium ratio, and $CaCl_2$ content on the particle size were also determined. The addition of methanol led to larger particles, while the increase of the other two parameters allowed the formation of smaller particles. The increase of these three parameters reduced the solid waste generated from the reaction, meaning higher calcium conversions. Methanol is crucial for the solubilization of lime. It is supposed that methanol mainly locates at two sites: the polar core of reverse micelles and the interfacial zone of the surfactant layer plays as a cosurfactant and markedly reduces the rigidity of micelles [216].

4. Conclusions

In this review article, the carbonation approach for the synthesis of $CaCO_3$ was summarized. The process mechanism, as well as the effect of the operating parameters on the properties of calcium carbonate (size, shape and polymorphism) were described. Parameters such as supersaturation, temperature, pH, Ca^{2+}/CO_3^{2-} ratio and flow regime play an important role in the $CaCO_3$ crystallization process through carbonation. High supersaturation, high pH values, and low temperatures favor the synthesis of calcite crystals. In these conditions, the Ca^{2+}/CO_3^{2-} ratio can significantly affect the crystal growth habit of the calcite crystals, modifying the morphology of the product. Conversely, low supersaturation, low pH values, low temperatures, and low Ca^{2+}/CO_3^{2-} ratios lead to the synthesis of vaterite crystals. Instead, high temperatures are determinant to synthesize aragonite crystals. The flow regime can determine the crystal size, directly affecting the CO_2 absorption rate, the controlling step in the carbonation-precipitation process.

The particle properties can be tailored for a determined final application by using some additives like NH_4^+ ions, Mg^{2+} ions and surfactants in order to control the size, shape and polymorphism of $CaCO_3$.

Concerning the reactor aspects, besides traditional and established apparatus like gas-liquid contactors and bubble columns, novel experimental setups exploiting process intensification techniques, such as rotating packed bed or microstructure minireactors, have been employed. These techniques avoid segregation issues and improve the CO_2 absorption and micromixing, allowing the synthesis of nanoparticles with narrow PSD, the achievement of higher CO_2 conversions as well as $CaCO_3$ particles with tailored properties. However, these intensified processes still lie on a laboratory scale, and further investigations are needed to reach an industrial level.

In conclusion, the synthesis of $CaCO_3$ through the carbonation route is a continuously growing field of research, since it is a simple and versatile process providing sub-micrometric and nanometric material with high purity, suitable to be employed in several applications. Besides, it is a high potential process for the reuse of industrial wastes and mitigation of CO_2 in a circular-economy approach. In this framework, a lot of work has been done as a wide range of industrial Ca-rich wastes have already been tested, and the operating parameters have been varied and optimized in order to obtain sub-micrometric $CaCO_3$ particles. Further studies are required in this field, such as the possibility of producing valuable $CaCO_3$ particles starting directly from flue gases containing CO_2, thus reducing or avoiding the very expensive purification steps. From a point of view of process intensification, current techniques should be deeply studied in order to bring these technologies to a larger scale. The aim of these studies should be the reduction of the high-energy intensity of the process. The current achievements and efforts are promising and indicate that this technology can be industrially applied, thus allowing CO_2 emissions mitigation.

Declaration of Competing Interest

The authors declare that they have no known competing financial interests or personal relationships that could have appeared to influence the work reported in this paper.

Acknowledgements

This project has received funding from the European Union's Horizon 2020 Research and Innovation Programme under Grant Agreement No. 768583. This paper reflects only the author's view and the content is the sole responsibility of the authors. The European Commission or its services cannot be held responsible for any use that may be made of the information it contains.

References

[1] K. Simkiss, Variations in the crystalline form of calcium carbonate precipitated from artificial sea water, Nature. 201 (1964) 492–493, https://doi.org/10.1038/201492a0.
[2] A. Declet, E. Reyes, O.M. Suárez, Calcium carbonate precipitation: a review of the carbonate crystallization process and applications in bioinspired composites, Rev. Adv. Mater. Sci. 44 (2016) 87–107.
[3] J.D. Rodriguez-Blanco, S. Shaw, L.G. Benning, The kinetics and mechanisms of amorphous calcium carbonate (ACC) crystallization to calcite, via vaterite, Nanoscale. 3 (2011) 265–271, https://doi.org/10.1039/c0nr00589d.
[4] P. Bots, L.G. Benning, J.D. Rodriguez-Blanco, T. Roncal-Herrero, S. Shaw, Mechanistic insights into the crystallization of amorphous calcium carbonate (ACC), Cryst. Growth Des. 12 (2012) 3806–3814, https://doi.org/10.1021/cg300676b.
[5] F. Liendo, M. Arduino, F.A. Deorsola, S. Bensaid, Optimization of $CaCO_3$ synthesis through the carbonation route in a packed bed reactor, Powder Technol. 377 (2021)https://doi.org/10.1016/j.powtec.2020.09.036.
[6] Z. Hu, M. Shao, Q. Cai, S. Ding, C. Zhong, X. Wei, Y. Deng, Synthesis of needle-like aragonite from limestone in the presence of magnesium chloride, J. Mater. Process. Technol. 209 (2009) 1607–1611, https://doi.org/10.1016/j.jmatprotec.2008.04.008.
[7] B. Jones, Review of calcium carbonate polymorph precipitation in spring systems, Sediment. Geol. 353 (2017) 64–75, https://doi.org/10.1016/j.sedgeo.2017.03.006.
[8] R. Chang, D. Choi, M.H. Kim, Y. Park, Tuning crystal polymorphisms and structural investigation of precipitated calcium carbonates for CO_2 mineralization, ACS Sustain. Chem. Eng. 5 (2017) 1659–1667, https://doi.org/10.1021/acssuschemeng.6b02411.
[9] M. Wang, H.K. Zou, L. Shao, J.F. Chen, Controlling factors and mechanism of preparing needlelike $CaCO_3$ under high-gravity environment, Powder Technol. 142 (2004) 166–174, https://doi.org/10.1016/j.powtec.2004.05.003.
[10] Z. Hu, Y. Deng, Synthesis of needle-like aragonite from calcium chloride and sparingly soluble magnesium carbonate, Powder Technol. 140 (2004) 10–16, https://doi.org/10.1016/j.powtec.2004.01.001.
[11] I. Udrea, C. Capat, E.A. Olaru, R. Isopescu, M. Mihai, C.D. Mateescu, C. Bradu, Vaterite synthesis via gas-liquid route under controlled pH conditions, Ind. Eng. Chem. Res. 51 (2012) 8185–8193, https://doi.org/10.1021/ie202221m.
[12] Q. Hu, J. Zhang, H. Teng, U. Becker, Growth process and crystallographic properties of ammonia-induced vaterite, Am. Mineral. 97 (2012) 1437–1445, https://doi.org/10.2138/am.2012.3983.
[13] B. Wang, Z. Pan, H. Cheng, Z. Chen, F. Cheng, High-yield synthesis of vaterite microparticles in gypsum suspension system via ultrasonic probe vibration/magnetic stirring, J. Cryst. Growth 492 (2018) 122–131, https://doi.org/10.1016/j.jcrysgro.2018.02.021.
[14] J. Harris, S.E. Wolf, Desiccator volume: a vital yet ignored parameter in $CaCO_3$ crystallization by the ammonium carbonate diffusion method, Minerals. 7 (2017) https://doi.org/10.3390/min7070122.
[15] K.J. Davis, P.M. Dove, J.J. De Yoreo, The role of Mg^{2+} as an impurity in calcite growth, Science (80-.) 290 (2000) 1134–1137, https://doi.org/10.1126/science.290.5494.1134.
[16] J. Kawano, N. Shimobayashi, A. Miyake, M. Kitamura, Precipitation diagram of calcium carbonate polymorphs: its construction and significance, J. Phys. Condens. Matter 21 (2009)https://doi.org/10.1088/0953-8984/21/42/425102.
[17] D.B. Trushina, T.V. Bukreeva, M.V. Kovalchuk, M.N. Antipina, $CaCO_3$ vaterite microparticles for biomedical and personal care applications, Mater. Sci. Eng. C 45 (2014) 644–658, https://doi.org/10.1016/j.msec.2014.04.050.
[18] Y.I. Svenskaya, H. Fattah, O.A. Inozemtseva, A.G. Ivanova, S.N. Shtykov, D.A. Gorin, B.V. Parakhonskiy, Key parameters for size- and shape-controlled synthesis of vaterite particles, Cryst. Growth Des. 18 (2018) 331–337, https://doi.org/10.1021/acs.cgd.7b01328.
[19] Y. Boyjoo, V.K. Pareek, J. Liu, Synthesis of micro and nano-sized calcium carbonate particles and their applications, J. Mater. Chem. A 2 (2014) 14270–14288, https://doi.org/10.1039/c4ta02070g.
[20] C.W. Hargis, A. Telesca, P.J.M. Monteiro, Calcium sulfoaluminate (Ye'elimite) hydration in the presence of gypsum, calcite, and vaterite, Cem. Concr. Res. 65 (2014) 15–20, https://doi.org/10.1016/j.cemconres.2014.07.004.
[21] I. Alvin, L. Porter, S. John, J. Wilson, S. John, Manufacture of Precipitated Calcium Carbonate of Improved Color and Stable Crystalline Form, 2000.
[22] M. Devenney, M. Fernandez, S.O. Morgan, Non-cementitious Compositions Comprising Vaterite and Methods Thereof, 2015.
[23] Z.-G. Cui, C.-F. Cui, Y. Zhu, B.P. Binks, Multiple phase inversion of emulsions stabilized by in situ surface activation of $CaCO_3$ nanoparticles via adsorption of fatty acids, Langmuir. 28 (2012) 314–320, https://doi.org/10.1021/la204021v.
[24] S. Liu, Stabilized Vaterite, 2003.

[25] M.-G. Ma, R.-C. Su, Biomineralization and biomimetic synthesis of biomineral and nanomaterials, Adv. Biomimetics (2011)https://doi.org/10.5772/13838.

[26] H. Ohgushi, M. Okumura, T. Yoshikawa, K. Inboue, N. Senpuku, S. Tamai, E.C. Shors, Bone formation processin porous calcium carbonate and hydroxyapatite, J. Biomed. Mater. Res. 26 (1992) 885–895, https://doi.org/10.1002/jbm.820260705.

[27] J. Nakamura, G. Poologasundarampillai, J.R. Jones, T. Kasuga, Tracking the formation of vaterite particles containing aminopropyl-functionalized silsesquioxane and their structure for bone regenerative medicine, J. Mater. Chem. B 1 (2013) 4446–4454, https://doi.org/10.1039/C3TB20589D.

[28] T.V. Bukreeva, I.V. Marchenko, T.N. Borodina, I.V. Degtev, S.L. Sitnikov, Y.V. Moiseeva, N.V. Gulyaeva, M.V. Kovalchuk, Calcium carbonate and titanium dioxide particles as a basis for container fabrication for brain delivery of compounds, Dokl. Phys. Chem. 440 (2011) 165–167, https://doi.org/10.1134/S001250161109003X.

[29] J. Camiletti, A.M. Soliman, M.L. Nehdi, Effects of nano- and micro-limestone addition on early-age properties of ultra-high-performance concrete, Mater. Struct. Constr. 46 (2013) 881–898, https://doi.org/10.1617/s11527-012-9940-0.

[30] C. Ramakrishna, T. Thenepalli, J.W. Ahn, A brief review of aragonite precipitated calcium carbonate (PCC) synthesis methods and its applications, Korean Chem. Eng. Res. 55 (2017) 443–455, https://doi.org/10.9713/kcer.2017.55.4.443.

[31] W.K. Park, S.J. Ko, S.W. Lee, K.H. Cho, J.W. Ahn, C. Han, Effects of magnesium chloride and organic additives on the synthesis of aragonite precipitated calcium carbonate, J. Cryst. Growth 310 (2008) 2593–2601, https://doi.org/10.1016/j.jcrysgro.2008.01.023.

[32] R.M. Santos, P. Ceulemans, T. Van Gerven, Synthesis of pure aragonite by sonochemical mineral carbonation, Chem. Eng. Res. Des. 90 (2012) 715–725, https://doi.org/10.1016/j.cherd.2011.11.022.

[33] M. Altiner, M. Yildirim, Production and characterization of synthetic aragonite prepared from dolomite by eco-friendly leaching–carbonation process, Adv. Powder Technol. 28 (2017) 553–564, https://doi.org/10.1016/j.apt.2016.10.024.

[34] N. Akilal, F. Lemaire, N.B. Bercu, S. Sayen, S.C. Gangloff, Y. Khelfaoui, H. Rammal, H. Kerdjoudj, Cowries derived aragonite as raw biomaterials for bone regenerative medicine, Mater. Sci. Eng. C 94 (2019) 894–900, https://doi.org/10.1016/j.msec.2018.10.039.

[35] Z. Hu, M. Shao, H. Li, Q. Cai, C. Zhong, Z. Xianming, Y. Deng, Synthesis of needle-like aragonite crystals in the presence of magnesium chloride and their application in papermaking, Adv. Compos. Mater. 18 (2009) 315–326, https://doi.org/10.1163/156855109X434720.

[36] M.A. Hubbe, R.A. Gill, Filler for papermaking: A review of their properties, and their mechanism role, Bioresorces. 11 (2016) 2886–2963.

[37] E.S. Place, N.D. Evans, M.M. Stevens, Complexity in biomaterials for tissue engineering, Nat. Mater. 8 (2009) 457–470, https://doi.org/10.1038/nmat2441.

[38] A. Rupani, L.A. Hidalgo-Bastida, F. Rutten, A. Dent, I. Turner, S. Cartmell, Osteoblast activity on carbonated hydroxyapatite, J. Biomed. Mater. Res. - Part A. 100 (A) (2012) 1089–1096, https://doi.org/10.1002/jbm.a.34037.

[39] G.H. Fairchild, R.L. Thatcher, Acicular Calcite and Aragonite Calcium Carbonate, 6071336, 2000.

[40] Shang Wenyu, Liu Qingfeng, Enguang He, Chen Shoutian, Study on properties of polymers packed by aragonite whisker, Proc. 6th Int. Conf. Prop. Appl. Dielectr. Mater. (Cat. No.00CH36347), vol.1, 2000, pp. 431–434, https://doi.org/10.1109/ICPADM.2000.875722.

[41] Y. Ding, Y. Liu, Y. Ren, H. Yan, M. Wang, D. Wang, X.Y. Lu, B. Wang, T. Fan, H. Guo, Controllable synthesis of all the anhydrous $CaCO_3$ polymorphs with various morphologies in $CaCl_2$-NH_3-CO_2 aqueous system, Powder Technol. 333 (2018) 410–420, https://doi.org/10.1016/j.powtec.2018.04.056.

[42] C.Y. Tai, F.B. Chen, Polymorphism of $CaCO_3$ precipitated in a constant-composition environment, AlCHE J. 44 (1998) 1790–1798, https://doi.org/10.1002/aic.690440810.

[43] B.J. Kim, E.H. Park, K.D. Choi, K.S. Kang, Synthesis of $CaCO_3$ using CO_2 at room temperature and ambient pressure, Mater. Lett. 190 (2017) 45–47, https://doi.org/10.1016/j.matlet.2016.12.030.

[44] Y.S. Han, G. Hadiko, M. Fuji, M. Takahashi, Effect of flow rate and CO_2 content on the phase and morphology of $CaCO_3$ prepared by bubbling method, J. Cryst. Growth 276 (2005) 541–548, https://doi.org/10.1016/j.jcrysgro.2004.11.408.

[45] B. Sun, X. Wang, J. Chen, G. Chu, J. Chen, L. Shao, Synthesis of nano-$CaCO_3$ by simultaneous absorption of CO_2 and NH_3 into $CaCl_2$ solution in a rotating packed bed, Chem. Eng. J. 168 (2011) 731–736, https://doi.org/10.1016/j.cej.2011.01.068.

[46] Z. Jia, Q. Chang, J. Qin, A. Mamat, Preparation of calcium carbonate nanoparticles with a continuous gas-liquid membrane contactor: particles morphology and membrane fouling, Chin. J. Chem. Eng. 21 (2013) 121–126, https://doi.org/10.1016/S1004-9541(13)60449-8.

[47] M. Altiner, Influences of CO2 bubbling types on preparation of calcite nanoparticles by carbonation process, Period. Polytech. Chem. Eng. 62 (2018) 209–214, https://doi.org/10.3311/PPch.10664.

[48] T. Thriveni, J.W. Ahn, C. Ramakrishna, Y.J. Ahn, C. Han, Synthesis of nano precipitated calcium carbonate by using a carbonation process through a closed loop reactor, J. Korean Phys. Soc. 68 (2016) 131–137, https://doi.org/10.3938/jkps.68.131.

[49] C. Domingo, E. Loste, J. Gómez-Morales, J. García-Carmona, J. Fraile, Calcite precipitation by a high-pressure CO_2 carbonation route, J. Supercrit. Fluids 36 (2006) 202–215, https://doi.org/10.1016/J.SUPFLU.2005.06.006.

[50] A.R. Ibrahim, J.B. Vuningoma, Y. Huang, H. Wang, J. Li, Rapid carbonation for calcite from a solid-liquid-gas system with an imidazolium-based ionic liquid, Int. J. Mol. Sci. 15 (2014) 11350–11363, https://doi.org/10.3390/ijms150711350.

[51] G. Montes-Hernandez, F. Renard, N. Geoffroy, L. Charlet, J. Pironon, Calcite precipitation from CO_2-H_2O-$Ca(OH)_2$ slurry under high pressure of CO_2, J. Cryst. Growth 308 (2007) 228–236, https://doi.org/10.1016/j.jcrysgro.2007.08.005.

[52] Y. Wen, L. Xiang, Y. Jin, Synthesis of plate-like calcium carbonate via carbonation route, Mater. Lett. 57 (2003) 2565–2571, https://doi.org/10.1016/S0167-577X(02)01312-5.

[53] S.R. Shirsath, S.H. Sonawane, D.R. Saini, A.B. Pandit, Continuous precipitation of calcium carbonate using sonochemical reactor, Ultrason. Sonochem. 24 (2015) 132–139, https://doi.org/10.1016/j.ultsonch.2014.12.003.

[54] R. Isopescu, M. Mihai, C. Orbeci, D. Turtoi, Calcium carbonate precipitation through carbon dioxide chemisorption from flue gas into lime Suspension, Rev. Chim. 65 (2014) 1490–1494.

[55] I. Cosentino, L. Restuccia, G.A. Ferro, F. Liendo, F. Deorsola, S. Bensaid, Evaluation of the mechanical properties of cements with fillers derived from the CO_2 reduction of cement plants, Procedia Struct. Integr. 18 (2019) 472–483, https://doi.org/10.1016/J.PROSTR.2019.08.189.

[56] M. d'Amora, F. Liendo, F.A. Deorsola, S. Bensaid, S. Giordani, Toxicological profile of calcium carbonate nanoparticles for industrial applications, Colloids Surf. B: Biointerfaces (2020), 110947https://doi.org/10.1016/J.COLSURFB.2020.110947.

[57] S. Wardhani, F. Prasetia, M.M. Khunur, D. Purwonugroho, Y.P. Prananto, Effect of CO_2 flow rate and carbonation temperature in the synthesis of crystalline precipitated calcium carbonate (PCC) from limestone, Indones. J. Chem. 18 (2018) 573–579, https://doi.org/10.22146/ijc.26608.

[58] E. Ulkeryildiz, S. Kilic, E. Ozdemir, Nano-$CaCO_3$ synthesis by jet flow, Colloids Surf. A Physicochem. Eng. Asp. 512 (2017) 34–40, https://doi.org/10.1016/j.colsurfa.2016.10.037.

[59] M.Y. Memar, K. Adibkia, S. Farajnia, H.S. Kafil, S. Maleki-Diza, R. Ghotaslou, Biocompatibility, cytotoxicity and antimicrobial effects of gentamicin-loaded $CaCO_3$ as a drug delivery to osteomyelitis, J. Drug Deliv. Sci. Technol. 54 (2019), 101307https://doi.org/10.1016/j.jddst.2019.101307.

[60] Y. Fujita, T. Yamamuro, T. Nakamura, S. Kotani, C. Ohtsuki, T. Kokubo, The bonding behavior of calcite to bone, J. Biomed. Mater. Res. 25 (1991) 991–1003, https://doi.org/10.1002/jbm.820250806.

[61] E. Khoozani, Bahrololoom, Bagheri, Modification of a soft drink by adding calcium carbonate nanoparticles to prevent tooth erosion, J. Dent. Biomater. 1 (2014) 38–44.

[62] E. Ulkeryildiz, S. Kilic, E. Ozdemir, Rice-like hollow nano-$CaCO_3$ synthesis, J. Cryst. Growth 450 (2016) 174–180, https://doi.org/10.1016/j.jcrysgro.2016.06.032.

[63] T. Jensdottir, A. Bardow, P. Holbrook, Properties and modification of soft drinks in relation to their erosive potential in vitro, J. Dent. 33 (2005) 569–575, https://doi.org/10.1016/j.jdent.2004.12.002.

[64] S.M. Dizaj, M. Barzegar-Jalali, M. Hossein Zarrintan, K. Adibkia, F. Lotfipour, Calcium carbonate nanoparticles; potential in bone and tooth disorders, Pharm. Sci. 20 (2015) 175–182, https://doi.org/10.5681/PS.2015.008.

[65] M. Hannig, C. Hannig, Nanotechnology and its role in caries therapy, Adv. Dent. Res. 24 (2012) 53–57, https://doi.org/10.1177/0022034512450446.

[66] J.A. Cury, S.B. Francisco, G.S. Simões, A.A. Del Bel Cury, C.P.M. Tabchoury, Effect of a calcium carbonate-based dentifrice on enamel demineralization in situ, Caries Res. 37 (2003) 194–199, https://doi.org/10.1159/000070444.

[67] M. Ma, Y. Yan, C. Qi, S. Qi, S. Chern, G. Shang, R. Wang, H. Chen, Symmetry-breaking assembled porous calcite microspheres and their multiple dental applications, Sci. China Mater. 60 (2017) 516–528, https://doi.org/10.1007/s40843-017-9038-5.

[68] L. Li, Y. Yang, Y. Lv, P. Yin, T. Lei, Porous calcite $CaCO_3$ microspheres: preparation, characterization and release behavior as doxorubicin carrier, Colloids Surf. B: Biointerfaces 186 (2020)https://doi.org/10.1016/j.colsurfb.2019.110720.

[69] X. Ma, L. Li, L. Yang, C. Su, Y. Guo, K. Jiang, Preparation of highly ordered hierarchical CaCO3 hemisphere and the application as pH value-sensitive anticancer drug carrier, Mater. Lett. 65 (2011) 3176–3179, https://doi.org/10.1016/j.matlet.2011.07.009.

[70] Y. Ueno, H. Futagawa, Y. Takagi, A. Ueno, Y. Mizushima, Drug-incorporating calcium carbonate nanoparticles for a new delivery system, J. Control. Release 103 (2005) 93–98, https://doi.org/10.1016/j.jconrel.2004.11.015.

[71] F. Monchau, P. Hivart, B. Genestie, F. Chai, M. Descamps, H.F. Hildebrand, Calcite as a bone substitute. Comparison with hydroxyapatite and tricalcium phosphate with regard to the osteoblastic activity, Mater. Sci. Eng. C 33 (2013) 490–498, https://doi.org/10.1016/j.msec.2012.09.019.

[72] M.M. Walker, J.L. Katz, Evaluation of bonding of bone to inorganic crystal surfaces, Bull. Hosp. Jt. Dis. Orthop. Inst. 43 (1983) 103–108.

[73] R.E. Holmes, E.C. Shors, G. Kopchok, L.R. Kitabayashi, R.T. Laborde, Effect of implant biodegradation rate on bone repair, Trans. 26th Ann. Meet. Sot. Biornat. 1990, p. 290.

[74] T. Sato, J.J. Beaudoin, Effect of nano-$CaCO_3$ on hydration of cement containing supplementary cementitious materials, Adv. Cem. Res. 23 (2011) 33–43, https://doi.org/10.1680/adcr.9.00016.

[75] T. Sato, F. Diallo, Seeding effect of nano-$CaCO_3$ on the hydration of tricalcium silicate, Transp. Res. Rec. (2010) 61–67, https://doi.org/10.3141/2141-11.

[76] C. Maier, T. Calafut, C. Maier, T. Calafut, Fillers and reinforcements, Polypropylene 1998, pp. 49–56, https://doi.org/10.1016/B978-188420758-7.50009-6.

[77] K. Palanikumar, R. Ashokgandhi, B.K. Raghunath, V. Jayaseelan, Role of Calcium Carbonate ($CaCO_3$) in improving wear resistance of Polypropylene (PP) components used in automobiles, Mater. Today Proc. 16 (2019) 1363–1371, https://doi.org/10.1016/j.matpr.2019.05.237.

[78] Y. Li, Q.F. Fang, Z.G. Yi, K. Zheng, A study of internal friction in polypropylene (PP) filled with nanometer-scale CaCO 3 particles, Mater. Sci. Eng. A (2004) 268–272, https://doi.org/10.1016/j.msea.2003.07.014.

[79] G. Vigier, Y. Bomal, G. Orange, T. Labour, C. Gauthier, R. Se, Infuence of the β crystalline phase on the mechanical properties of un filled and $CaCO_3$-filled polypropylene. I. Structural and mechanical characterisation, Polymer 42 (2001) 7127–7135.

[80] Z. Bartczak, A.S. Argon, R.E. Cohen, M. Weinberg, Toughness mechanism in semi-crystalline polymer blends: II. High-density polyethylene toughened with calcium carbonate filler particles, Polymer 40 (1999) 2347–2365.

[81] R.S. Somani, K.S. Patel, A.R. Mehta, R.V. Jasra, Examination of the polymorphs and particle size of calcium carbonate precipitated using still effluent (i.e., $CaCl_2$ + NaCl solution) of soda ash manufacturing process, Ind. Eng. Chem. Res. 45 (2006) 5223–5230, https://doi.org/10.1021/ie0513447.

[82] G.J. Price, M.F. Mahon, J. Shannon, C. Cooper, Composition of calcium carbonate polymorphs precipitated using ultrasound, Cryst. Growth Des. 11 (2011) 39–44, https://doi.org/10.1021/cg901240n.

[83] P.-C. Chen, C.Y. Tai, K.C. Lee, Morphology and growth rate of calcium carbonate crystals in a gas-liquid-solid reactive crystallizer, Chem. Eng. Sci. 52 (1997) 4171–4177, https://doi.org/10.1016/S0009-2509(97)00259-5.

[84] C. Ra, T. Thenepalli, J.H. Huh, J.W. Ahn, Precipitated calcium carbonate synthesis by simultaneous injection to produce nano whisker aragonite, J. Korean Ceram. Soc. 53 (2016) 222–226, https://doi.org/10.4191/kcers.2016.53.2.222.

[85] R. Faivre, Recherche des conditions physico-chimiques de précipitation des trois formes crystallines du carbonate de calcium préparé par double decomposition du chlorure de calcium et du carbonate de sodium, Compt. Rend. 222 (1946) 140–141.

[86] Y. Kitano, A study of the polymorphic formation of calcium carbonate in thermal springs with an emphasis on the effect of temperature, Bull. Chem. Soc. Jpn. 35 (1962) 1980–1985, https://doi.org/10.1246/bcsj.35.1980.

[87] G.T. Zhou, J.C. Yu, X.C. Wang, L.Z. Zhang, Sonochemical synthesis of aragonite-type calcium carbonate with different morphologies, New J. Chem. 28 (2004) 1027–1031, https://doi.org/10.1039/b315198k.

[88] X. Luo, X. Song, Y. Cao, L. Song, X. Bu, Investigation of calcium carbonate synthesized by steamed ammonia liquid waste without use of additives, RSC Adv. 10 (2020) 7976–7986, https://doi.org/10.1039/c9ra10460g.

[89] J. Prah, J. MačEk, G. Dražič, Precipitation of calcium carbonate from a calcium acetate and ammonium carbamate batch system, J. Cryst. Growth 324 (2011) 229–234, https://doi.org/10.1016/j.jcrysgro.2011.03.020.

[90] Z. Nan, Q. Yang, Z. Chen, Novel morphologies and phase transformation of $CaCO_3$ crystals formed in CDS and urea aqueous solution, J. Cryst. Growth 312 (2010) 705–713, https://doi.org/10.1016/j.jcrysgro.2009.12.044.

[91] D. Konopacka-Łyskawa, Synthesis methods and favorable conditions for spherical vaterite precipitation: a review, Crystals. 9 (2019)https://doi.org/10.3390/cryst9040223.

[92] K. Gorna, M. Hund, M. Vučak, F. Gröhn, G. Wegner, Amorphous calcium carbonate in form of spherical nanosized particles and its application as fillers for polymers, Mater. Sci. Eng. A 477 (2008) 217–225, https://doi.org/10.1016/j.msea.2007.05.045.

[93] M. Dietzsch, I. Andrusenko, R. Branscheid, F. Emmerling, U. Kolb, W. Tremel, Snapshots of calcium carbonate formation - a step by step analysis, Zeitschrift Fur Krist. - Cryst. Mater. 232 (2017) 255–265, https://doi.org/10.1515/zkri-2016-1973.

[94] J. Liu, S. Pancera, V. Boyko, J. Gummel, R. Nayuk, K. Huber, Impact of sodium polyacrylate on the amorphous calcium carbonate formation from supersaturated solution, Langmuir. 28 (2012) 3593–3605, https://doi.org/10.1021/la203895d.

[95] K. Mohamadzadeh-Saghavaz, H. Resalati, A. Ghasemian, Cellulose-precipitated calcium carbonate composites and their effect on paper properties, Chem. Pap. 68 (2014) 774–781, https://doi.org/10.2478/s11696-013-0513-7.

[96] P. Anbu, C.H. Kang, Y.J. Shin, J.S. So, Formations of calcium carbonate minerals by bacteria and its multiple applications, Springerplus. (2016) 1–26, https://doi.org/10.1186/s40064-016-1869-2.

[97] S.P. Chaparro-Acuña, L. Becerra-Jiménez, J. Jobanny Martínez-Zambrano, H.A. Rojas-Sarmiento, Soil bacteria that precipitate calcium carbonate: mechanism and applications of the process Bacterias del suelo que precipitan carbonato de calcio: mecanismo y aplicaciones del proceso, Acta Agron. 67 (2018) 277–288, https://doi.org/10.15446/acag.v67n2.66109.

[98] B. Krajewska, Urease-aided calcium carbonate mineralization for engineering applications: a review, J. Adv. Res. 13 (2018) 59–67, https://doi.org/10.1016/j.jare.2017.10.009.

[99] C.M. Gorospe, S.H. Han, S.G. Kim, J.Y. Park, C.H. Kang, J.H. Jeong, J.S. So, Effects of different calcium salts on calcium carbonate crystal formation by Sporosarcina pasteurii KCTC 3558, Biotechnol, Bioprocess Eng. 18 (2013) 903–908, https://doi.org/10.1007/s12257-013-0030-0.

[100] A.W. Xu, Q. Yu, W.F. Dong, M. Antonietti, H. Cölfen, Stable amorphous $CaCO_3$ microparticles with hollow spherical superstructures stabilized by phytic acid, Adv. Mater. 17 (2005) 2217–2221, https://doi.org/10.1002/adma.200500747.

[101] P.K. Ajikumar, G.W. Ling, G. Subramanyam, R. Lakshminarayanan, S. Valiyaveettil, Synthesis and characterization of monodispersed spheres of amorphous calcium carbonate and calcite spherules, Cryst. Growth Des. 5 (2005) 1129–1134, https://doi.org/10.1021/cg049606f.

[102] X.H. Guo, S.H. Yu, G.B. Cai, Crystallization in a mixture of solvents by using a crystal modifier: morphology control in the synthesis of highly monodisperse $CaCO_3$ microspheres, Angew. Chem. Int. Ed. 45 (2006) 3977–3981, https://doi.org/10.1002/anie.200600029.

[103] A.W. Xu, M. Antonietti, S.H. Yu, H. Cölfen, Polymer-mediated mineralization and self-similar mesoscale-organized calcium carbonate with unusual superstructures, Adv. Mater. 20 (2008) 1333–1338, https://doi.org/10.1002/adma.200701723.

[104] D. Liu, M.Z. Yates, Formation of rod-shaped calcite crystals by microemulsion-based synthesis, Langmuir. 22 (2006) 5566–5569, https://doi.org/10.1021/la060612i.

[105] S. Thachepan, M. Li, S.A. Davis, S. Mann, Additive-mediated crystallization of complex calcium carbonate superstructures in reverse microemulsions, Chem. Mater. 18 (2006) 3557–3561, https://doi.org/10.1021/cm060847f.

[106] C.Y. Tai, C. Kuang Chen, Particle morphology, habit, and size control of $CaCO_3$ using reverse microemulsion technique, Chem. Eng. Sci. 63 (2008) 3632–3642, https://doi.org/10.1016/j.ces.2008.04.022.

[107] C.K. Chen, C.Y. Tai, Competing effects of operating variables in the synthesis of $CaCO_3$ particles using the reverse microemulsion technique, Chem. Eng. Sci. 65 (2010) 4761–4770, https://doi.org/10.1016/j.ces.2010.05.019.

[108] R.K. Pai, S. Pillai, Nanoparticles of amorphous calcium carbonate by miniemulsion: synthesis and mechanism, CrystEngComm. 10 (2008) 865–872, https://doi.org/10.1039/b717057b.

[109] Y. Fukui, K. Fujimoto, Bio-inspired nanoreactor based on a miniemulsion system to create organic-inorganic hybrid nanoparticles and nanofilms, J. Mater. Chem. 22 (2012) 3493–3499, https://doi.org/10.1039/c2jm14661d.

[110] Y. Fukui, H. Takamatsu, K. Fujimoto, Creation of hybrid polymer particles through morphological tuning of $CaCO_3$ crystals in miniemulsion system, Colloids Surf. A Physicochem. Eng. Asp. 516 (2017) 1–8, https://doi.org/10.1016/j.colsurfa.2016.12.013.

[111] A.U. Badnore, A.B. Pandit, Synthesis of nanosized calcium carbonate using reverse miniemulsion technique: comparison between sonochemical and conventional method, Chem. Eng. Process. Process Intensif. 98 (2015) 13–21, https://doi.org/10.1016/j.cep.2015.10.003.

[112] M.V. Dagaonkar, A. Mehra, R. Jain, H.J. Heeres, Synthesis of $CaCO_3$ nanoparticles of lime solutions in reverse micellar systems, Chem. Eng. Res. Des. 82 (2004) 1438–1443.

[113] G. Huang, C.H. Lu, H.H. Yang, Magnetic nanomaterials for magnetic bioanalysis, Nov. Nanomater. Biomed. Environ. Energy Appl. 2019, pp. 89–109, https://doi.org/10.1016/B978-0-12-814497-8.00003-5.

[114] N.H. Sulimai, R.A. Rani, Z. Khusaimi, S. Abdullah, M.J. Salifairus, M. Rusop, S. Alrokayan, H. Khan, One step precipitation of CaCO3 nanoparticles assisted by drying and hydrothermal method, Proc. 2017 IEEE Reg. Symp. Micro Nanoelectron. RSM 2017 2017, pp. 187–190, https://doi.org/10.1109/RSM.2017.8069134.

[115] Z. Zhao, L. Zhang, H. Dai, Y. Du, X. Meng, R. Zhang, Y. Liu, J. Deng, Surfactant-assisted solvo- or hydrothermal fabrication and characterization of high-surface-area porous calcium carbonate with multiple morphologies, Microporous Mesoporous Mater. 138 (2011) 191–199, https://doi.org/10.1016/j.micromeso.2010.09.006.

[116] Y.X. Chen, X.B. Ji, Y.L. Quan, Solvothermal synthesis and characterization of hierarchical calcium carbonate spheres, Adv. Mater. Res. 912–914 (2014) 318–320, https://doi.org/10.4028/www.scientific.net/AMR.912-914.318.

[117] M.A. Karimi, M. Ranjbar, Hydrothermal synthesis and characterization of $CaCO_3$ nanostructure, Synth. React. Inorganic, Met. Nano-Metal Chem. 46 (2016) 635–637, https://doi.org/10.1080/15533174.2014.988817.

[118] J. Skubiszewska-Zięba, B. Charmas, H. Waniak-Nowicka, Hydrothermal and mechanochemical synthesis of crystalline $CaCO_3$, Adsorpt. Sci. Technol. 35 (2017) 668–676, https://doi.org/10.1177/0263617417704298.

[119] V.A. Juvekar, M.M. Sharma, Absorption of CO_2 in a suspension of lime, Chem. Eng. Sci. 28 (1973) 825–837, https://doi.org/10.1016/0009-2509(77)80017-1.

[120] H. Zhao, L. Shao, J.F. Chen, High-gravity process intensification technology and application, Chem. Eng. J. 156 (2010) 588–593, https://doi.org/10.1016/j.cej.2009.04.053.

[121] N. Czaplicka, The Overview of Reactors Used for the Production of Precipitated Calcium Carbonate via Carbonation Route, 2019.

[122] O.A. Jimoh, K.S. Ariffin, H. Bin Hussin, A.E. Temitope, Synthesis of precipitated calcium carbonate: a review, Carbonates Evaporites 33 (2018) 331–346, https://doi.org/10.1007/s13146-017-0341-x.

[123] Y. Liang, G. Chu, J. Wang, Y. Huang, J. Chen, B. Sun, L. Shao, Controllable preparation of nano-$CaCO_3$ in a microporous tube-in-tube microchannel reactor, Chem. Eng. Process. Process Intensif. 79 (2014) 34–39, https://doi.org/10.1016/j.cep.2014.03.006.

[124] M. Vučak, M.N. Pons, J. Perić, H. Vivier, Effect of precipitation conditions on the morphology of calcium carbonate: quantification of crystal shapes using image analysis, Powder Technol. 97 (1998) 1–5, https://doi.org/10.1016/S0032-5910(97)03375-5.

[125] D. Konopacka-Łyskawa, B. Kościelska, M. Łapiński, Precipitation of spherical vaterite particles via carbonation route in the bubble column and the gas-lift reactor, Jom. 71 (2019) 1041–1048, https://doi.org/10.1007/s11837-018-3307-0.

[126] H.P. Mattila, H. Hudd, R. Zevenhoven, Cradle-to-gate life cycle assessment of precipitated calcium carbonate production from steel converter slag, J. Clean. Prod. 84 (2014) 611–618, https://doi.org/10.1016/j.jclepro.2014.05.064.

[127] K. Zakuciová, V. Kočí, K. Ciahotný, A. Carvalho, J. Štefanica, J. Smutná, Life cycle assessment of calcium carbonate loop CO_2 capture technology for brown coal power plant unit of the Czech Republic, Comput. Aided. Chem. Eng. 43 (2018) 253–258, https://doi.org/10.1016/B978-0-444-64235-6.50045-0.

[128] H.H. Khoo, J. Bu, R.L. Wong, S.Y. Kuan, P.N. Sharratt, Carbon capture and utilization: preliminary life cycle CO2, energy, and cost results of potential mineral carbonation, Energy Procedia 4 (2011) 2494–2501, https://doi.org/10.1016/J.EGYPRO.2011.02.145.

[129] R. Chang, S. Kim, S. Lee, S. Choi, M. Kim, Y. Park, Calcium carbonate precipitation for CO_2 storage and utilization: a review of the carbonate crystallization and polymorphism, Front. Energy Res. 5 (2017) 1–12, https://doi.org/10.3389/fenrg.2017.00017.

[130] A. Sanna, M. Uibu, G. Caramanna, R. Kuusik, M.M. Maroto-Valer, A review of mineral carbonation technologies to sequester CO_2, Chem. Soc. Rev. 43 (2014) 8049–8080, https://doi.org/10.1039/c4cs00035h.

[131] E. Nduagu, J. Bergerson, R. Zevenhoven, Life cycle assessment of CO_2 sequestration in magnesium silicate rock – a comparative study, Energy Convers. Manag. 55 (2012) 116–126, https://doi.org/10.1016/J.ENCONMAN.2011.10.026.

[132] H.H. Khoo, P.N. Sharratt, J. Bu, T.Y. Yeo, A. Borgna, J.G. Highfield, T.G. Björklöf, R. Zevenhoven, Carbon capture and mineralization in singapore: preliminary environmental impacts and costs via LCA, Ind. Eng. Chem. Res. 50 (2011) 11350–11357, https://doi.org/10.1021/ie200592h.

[133] Y. Zhong, T. Shi, Q. Chen, X. Yang, D. Xu, Z. Zhang, X. Wang, B. Zhong, Leaching calcium from phosphogypsum desulfurization slag by using ammonium chloride solution: thermodynamics and kinetics study, Chin. J. Chem. Eng. 28 (2020) 208–215, https://doi.org/10.1016/j.cjche.2019.08.006.

[134] E.R. Bobicki, Q. Liu, Z. Xu, H. Zeng, Carbon capture and storage using alkaline industrial wastes, Prog. Energy Combust. Sci. 38 (2012) 302–320, https://doi.org/10.1016/j.pecs.2011.11.002.

[135] H.P. Mattila, R. Zevenhoven, Production of Precipitated Calcium Carbonate from Steel Converter Slag and Other Calcium-Containing Industrial Wastes and Residues, 1st ed Elsevier Inc., 2014https://doi.org/10.1016/B978-0-12-420221-4.00010-X.

[136] K. Song, W. Kim, J.H. Bang, S. Park, C.W. Jeon, Polymorphs of pure calcium carbonate prepared by the mineral carbonation of flue gas desulfurization gypsum, Mater. Des. 83 (2015) 308–313, https://doi.org/10.1016/j.matdes.2015.06.051.

[137] J. Jeon, M.J. Kim, CO_2 storage and $CaCO_3$ production using seawater and an alkali industrial by-product, Chem. Eng. J. 378 (2019), 122180https://doi.org/10.1016/j.cej.2019.122180.

[138] J.H. Bang, Y. Yoo, S.W. Lee, K. Song, S. Chae, CO_2 mineralization using brine discharged from a seawater desalination plant, Minerals. 7 (2017)https://doi.org/10.3390/min7110207.

[139] E. Batuecas, F. Liendo, T. Tommasi, S. Bensaid, F.A. Deorsola, D. Fino, Recycling CO_2 from flue gas for $CaCO_3$ nanoparticles production as cement filler: a life cycle assessment, J. CO2 Util. 45 (2021)https://doi.org/10.1016/j.jcou.2021.101446.

[140] N. Czaplicka, D. Konopacka-Łyskawa, P. Lewandowska, M. Łapiński, R. Bray, Influence of selected CO_2 absorption promoters on the characteristics of calcium carbonate particles produced by carbonation of the post-distillation liquid from the Solvay process, Powder Technol. 391 (2021) 432–441, https://doi.org/10.1016/j.powtec.2021.06.042.

[141] F.M. Baena-Moreno, M. Rodríguez-Galán, F. Vega, B. Alonso-Fariñas, L.F. Vilches Arenas, B. Navarrete, Carbon capture and utilization technologies: a literature review and recent advances, Energy Sources, Part A Recover. Util. Environ. Eff. 41 (2019) 1403–1433, https://doi.org/10.1080/15567036.2018.1548518.

[142] J. Sipilä, S. Teir, R. Zevenhoven, Carbon dioxide sequestration by mineral carbonation Literature review update 2005–2007, Rep. VT. (2008) 52, https://doi.org/10.1080/00908310600628263.

[143] R. Marin Rivera, T. Van Gerven, Production of calcium carbonate with different morphology by simultaneous CO_2 capture and mineralisation, J. CO2 Util. 41 (2020), 101241https://doi.org/10.1016/j.jcou.2020.101241.

[144] M.Y. Ryu, K.S. You, J.W. Ahn, H. Kim, Effect of the pH and basic additives on the precipitation of calcium carbonate during carbonation reaction, Resour. Process. 54 (2009) 14–18, https://doi.org/10.4144/rpsj.54.14.

[145] T.F. Hatch, R.L. Pigford, Simultaneous absorption of carbon dioxide and ammonia in water, Ind. Eng. Chem. Fundam. 1 (1962) 209–214, https://doi.org/10.1021/i160003a009.

[146] J. García Carmona, J. Gómez Morales, R. Rodríguez Clemente, Rhombohedral-scalenohedral calcite transition produced by adjusting the solution electrical conductivity in the system $Ca(OH)_2$-CO_2-H_2O, J. Colloid Interface Sci. 261 (2003) 434–440, https://doi.org/10.1016/S0021-9797(03)00149-8.

[147] C.Y. Tai, P.-C. Chen, S.-M. Shih, Size-dependent growth and contact nucleation of calcite crystals, AICHE J. 39 (1993) 1472–1482, https://doi.org/10.1002/aic.690390907.

[148] H.N.S. Wiechers, P. Sturrock, G.V.R. Marais, Calcium carbonate crystallization kinetics, Water Res. 9 (1975) 835–845, https://doi.org/10.1016/0043-1354(75)90143-8.

[149] J.P. Andreassen, M.J. Hounslow, Growth and aggregation of vaterite in seeded-batch experiments, AICHE J. 50 (2004) 2772–2782, https://doi.org/10.1002/aic.10205.

[150] S. Wachi, A.G. Jones, Mass transfer with chemical reaction and precipitation, Chem. Eng. Sci. 46 (1990) 1027–1033.

[151] D. Gómez-Díaz, J.M. Navaza, B. Sanjurjo, Analysis of mass transfer in the precipitation process of calcium carbonate using a gas/liquid reaction, Chem. Eng. J. 116 (2006) 203–209, https://doi.org/10.1016/j.cej.2005.12.004.

[152] I.C. Mayorga, J.M. Astilleros, L. Fernández-Díaz, Precipitation of $CaCO_3$ polymorphs from aqueous solutions: the role of ph and sulphate groups, Minerals. 9 (2019) 1–16, https://doi.org/10.3390/min9030178.

[153] A. Tamir, Y. Taitel, The effect of the gas side resistance on absorption with chemical reaction from binary mixtures, Chem. Eng. Sci. (1975)https://doi.org/10.1016/0009-2509(75)85025-1.

[154] L. Xiang, Y. Xiang, Y. Wen, F. Wei, Formation of $CaCO_3$ nanoparticles in the presence of terpineol, Mater. Lett. 58 (2004) 959–965, https://doi.org/10.1016/j.matlet.2003.07.034.

[155] A. Ataki, H.J. Bart, Experimental and CFD simulation study for the wetting of a structured packing element with liquids, Chem. Eng. Technol. 29 (2006) 336–347, https://doi.org/10.1002/ceat.200500302.

[156] C. Ramakrishna, T. Thenepalli, J.W. Ahn, Evaluation of various synthesis methods for calcite-precipitated calcium carbonate (PCC) formation, Korean Chem. Eng. Res. 55 (2017) 279–286, https://doi.org/10.9713/kcer.2017.55.3.279.

[157] B. Feng, A.K. Yong, H. An, Effect of various factors on the particle size of calcium carbonate formed in a precipitation process, Mater. Sci. Eng. A 445–446 (2007) 170–179, https://doi.org/10.1016/j.msea.2006.09.010.

[158] B. Zhou, B. Liu, H. Zou, Y. Song, L. Gong, Q. Huo, X. Xu, Y. Sheng, Facile synthesis of cubic and spindle-shaped $CaCO_3$ particles and their applications as red phosphor doped with Eu^{3+}, Colloids Surf. A Physicochem. Eng. Asp. 447 (2014) 166–171, https://doi.org/10.1016/j.colsurfa.2013.12.078.

[159] L.N. Schultz, M.P. Andersson, K.N. Dalby, D. Müter, D.V. Okhrimenko, H. Fordsmand, S.L.S. Stipp, High surface area calcite, J. Cryst. Growth 371 (2013) 34–38, https://doi.org/10.1016/j.jcrysgro.2013.01.049.

[160] S. Kilic, G. Toprak, E. Ozdemir, Stability of $CaCO_3$ in $Ca(OH)_2$ solution, Int. J. Miner. Process. (2016)https://doi.org/10.1016/j.minpro.2015.12.006.

[161] P.A. Hartley, G.D. Parfitt, L.B. Pollack, The role of the van der Waals force in the agglomeration of powders containing submicron particles, Powder Technol. 42 (1985) 35–46, https://doi.org/10.1016/0032-5910(85)80036-X.

[162] A.A. Esmailpour, R. Zarghami, N. Mostoufi, Effect of Temperature on the Nanoparticles Agglomerates Fluidization, 2015https://doi.org/10.2991/msam-15.2015.55.

[163] H. Liu, P. Lan, S. Lu, S. Wu, The crystallization kinetic model of nano-$CaCO_3$ in CO_2-ammonia-phosphogypsum three-phase reaction system, J. Cryst. Growth 492 (2018) 114–121, https://doi.org/10.1016/j.jcrysgro.2018.04.017.

[164] Y. Pan, X. Zhao, Y. Sheng, C. Wang, Y. Deng, X. Ma, Y. Liu, Z. Wang, Biomimetic synthesis of dendrite-shaped aragonite particles with single-crystal feature by polyacrylic acid, Colloids Surf. A Physicochem. Eng. Asp. 297 (2007) 198–202, https://doi.org/10.1016/j.colsurfa.2006.10.047.

[165] J. Gómez-Morales, J. Torrent-Burgués, A. López-Macipe, R. Rodríguez-Clemente, Precipitation of calcium carbonate from solutions with varying Ca^{2+} carbonate ratios, J. Cryst. Growth 166 (1996) 1020–1026, https://doi.org/10.1016/0022-0248(96)00083-8.

[166] N. Frikha, J. Sellami, H. Muhr, E. Plasari, Study on the Influence of Citrate Ion Concentration and Non-stoechiometric Ratio on the Crystal Growth Kinetics of Calcium Carbonate (Calcite), 2005.

[167] A.L. Smith, Electrokinetics of the oxide—solution interface, J. Colloid Interface Sci. 55 (1976) 525–530, https://doi.org/10.1016/0021-9797(76)90062-X.

[168] D.S. Cicerone, A.E. Regazzoni, M.A. Blesa, Electrokinetic properties of the calcite/water interface in the presence of magnesium and organic matter, J. Colloid Interface Sci. 154 (1992) 423–433, https://doi.org/10.1016/0021-9797(92)90158-I.

[169] M. He, E. Forssberg, Y. Wang, Y. Han, Ultrasonication-assisted synthesis of calcium carbonate nanoparticles, Chem. Eng. Commun. 192 (2005) 1468–1481, https://doi.org/10.1080/009864490896025.

[170] J.F. Chen, Y.H. Wang, F. Guo, X.M. Wang, C. Zheng, Synthesis of nanoparticles with novel technology: high-gravity reactive precipitation, Ind. Eng. Chem. Res. 39 (2000) 948–954, https://doi.org/10.1021/ie990549a.

[171] L. Ding, B. Wu, P. Luo, Preparation of $CaCO_3$ nanoparticles in a surface-aerated tank stirred by a long-short blades agitator, Powder Technol. 333 (2018) 339–346, https://doi.org/10.1016/j.powtec.2018.04.057.

[172] W.M. Jung, S. Hoon Kang, K.S. Kim, W.S. Kim, C. Kyun Choi, Precipitation of calcium carbonate particles by gasliquid reaction: morphology and size distribution of particles in Couette-Taylor and stirred tank reactors, J. Cryst. Growth 312 (2010) 3331–3339, https://doi.org/10.1016/j.jcrysgro.2010.08.026.

[173] I. Dalmolin, E. Skovroinski, A. Biasi, M.L. Corazza, C. Dariva, J.V. Oliveira, Solubility of Carbon Dioxide in Binary and Ternary Mixtures with Ethanol and Water, vol. 245, 2006 193–200, https://doi.org/10.1016/j.fluid.2006.04.017.

[174] L. Zhang, J.I. Siepmann, Direct calculation of Henry's law constants from Gibbs ensemble Monte Carlo simulations: nitrogen, oxygen, carbon dioxide and methane in ethanol, Theor. Chem. Accounts (2006) 391–397, https://doi.org/10.1007/s00214-005-0073-1.

[175] F. Liendo, M. Arduino, F.A. Deorsola, S. Bensaid, Optimization of $CaCO_3$ synthesis through the carbonation route in a packed bed reactor, Powder Technol. 377 (2021)https://doi.org/10.1016/j.powtec.2020.09.036.

[176] R. Santos, P. Ceulemans, D. François, T. Van Gerven, Ultrasound-enhanced mineral carbonation, Inst. Chem. Eng. Symp. Ser. 157 (2011) 108–116.

[177] A. Alamdari, A. Alamdari, D. Mowla, Kinetics of calcium carbonate precipitation through CO_2 absorption from flue gas into distiller waste of soda ash plant, J. Ind. Eng. Chem. 20 (2014) 3480–3486, https://doi.org/10.1016/j.jiec.2013.12.038.

[178] N. Czaplicka, D. Konopacka-Łyskawa, Studies on the utilization of post-distillation liquid from Solvay process to carbon dioxide capture and storage, SN Appl. Sci. 1 (2019) 1–8, https://doi.org/10.1007/s42452-019-0455-y.

[179] T. Ogino, T. Suzuki, K. Sawada, The rate and mechanism of polymorphic transformation of calcium carbonate in water, J. Cryst. Growth (1990)https://doi.org/10.1016/0022-0248(90)90618-U.

[180] J.H. Ahn, K.S. Choi, H. Kim, S.H. Yoon, J.S. Kim, G.W. Sung, K.H. Lee, Synthesis of aragonite by the carbonation process using stainless refining dust in iron & steel plants, Hydro Biohydrometall. 13 (C6) (2000) 29–36.

[181] G.T. Rochelle, Amine scrubbing for CO_2 capture, Science (80-.) 325 (2009) 1652–1654, https://doi.org/10.1126/science.1176731.

[182] D.N. Huntzinger, T.D. Eatmon, A life-cycle assessment of Portland cement manufacturing: comparing the traditional process with alternative technologies, J. Clean. Prod. 17 (2009) 668–675, https://doi.org/10.1016/J.JCLEPRO.2008.04.007.

[183] N. Czaplicka, D. Konopacka-Łyskawa, The Overview of Reactors Used for the Production of Precipitated Calcium Carbonate via Carbonation Route, 2019 245–250.

[184] D. Moutafchieva, D. Popova, M. Dimitrova, S. Tchaoushev, Experimental determination of the volumetric mass transfer coefficient, J. Univ. Chem. Technol. Metall. 48 (2013) 351–356.

[185] S. Kakaraniya, A. Gupta, A. Mehra, Reactive Precipitation in Gas-Slurry Systems: The CO 2 - Ca (OH) 2 - CaCO 3 System, 2007 3170–3179.

[186] M. Ukrainczyk, J. Kontrec, V. Babić-Ivančić, L. Brečević, D. Kralj, Experimental design approach to calcium carbonate precipitation in a semicontinuous process, Powder Technol. 171 (2007) 192–199, https://doi.org/10.1016/j.powtec.2006.10.046.

[187] R. Perry, S. Perry, D. Green, J. Maloney, Perry's Chemical Engineers' Handbook, 7th ed, 1997https://doi.org/10.1021/ed027p533.1.

[188] A.A. Yawalkar, A.B.M. Heesink, G.F. Versteeg, V.G. Pangarkar, Gas-liquid mass transfer coefficient in stirred tank reactors, Can. J. Chem. Eng. 80 (2008) 840–848, https://doi.org/10.1002/cjce.5450800507.
[189] S.S. Alves, C.I. Maia, J.M.T. Vasconcelos, A.J. Serralheiro, Bubble size in aerated stirred tanks, Chem. Eng. J. 89 (2002) 109–117, https://doi.org/10.1016/S1385-8947(02)00008-6.
[190] S. Alves, C. Maia, J.M. Vasconcelos, Experimental and modelling study of gas dispersion in a double turbine stirred tank, Chem. Eng. Sci. 57 (2002) 487–496, https://doi.org/10.1016/S0009-2509(01)00400-6.
[191] M. Kordač, V. Linek, Dynamic measurement of carbon dioxide volumetric mass transfer coefficient in a well-mixed reactor using a pH probe: analysis of the salt and supersaturation effects, Ind. Eng. Chem. Res. 47 (2008) 1310–1317, https://doi.org/10.1021/ie0711776.
[192] R.E. Treybal, in: Robert E. Treybal (Ed.), Mass-transfer operations, 2nd ed.McGraw-Hill Book Company, Inc., New York, 1955https://doi.org/10.1002/aic.690020430.
[193] J.H. Bang, Y.N. Jang, W. Kim, K.S. Song, C.W. Jeon, S.C. Chae, S.W. Lee, S.J. Park, M.G. Lee, Specific surface area and particle size of calcium carbonate precipitated by carbon dioxide microbubbles, Chem. Eng. J. 198–199 (2012) 254–260, https://doi.org/10.1016/j.cej.2012.05.081.
[194] B. Njegić-Džakula, G. Falini, L. Brečević, Ž. Skoko, D. Kralj, Effects of initial supersaturation on spontaneous precipitation of calcium carbonate in the presence of charged poly-l-amino acids, J. Colloid Interface Sci. 343 (2010) 553–563, https://doi.org/10.1016/J.JCIS.2009.12.010.
[195] W.H. Khan, V.K. Rathod, Process intensification approach for preparation of curcumin nanoparticles via solvent–nonsolvent nanoprecipitation using spinning disc reactor, Chem. Eng. Process. Process Intensif. 80 (2014) 1–10, https://doi.org/10.1016/J.CEP.2014.03.011.
[196] H. Cheng, X. Wang, B. Wang, J. Zhao, Y. Liu, F. Cheng, Effect of ultrasound on the morphology of the $CaCO_3$ precipitated from $CaSO_4$-NH_3-CO_2-H_2O system, J. Cryst. Growth 469 (2017) 97–105, https://doi.org/10.1016/j.jcrysgro.2016.10.017.
[197] Y. Luo, G.W. Chu, H.K. Zou, F. Wang, Y. Xiang, L. Shao, J.F. Chen, Mass transfer studies in a rotating packed bed with novel rotors: chemisorption of CO_2, Ind. Eng. Chem. Res. 51 (2012) 9164–9172, https://doi.org/10.1021/ie300466f.
[198] B.C. Sun, X.M. Wang, J.M. Chen, G.W. Chu, J.F. Chen, L. Shao, Synthesis of nano-$CaCO_3$ by simultaneous absorption of CO_2 and NH_3 into $CaCl_2$ solution in a rotating packed bed, Chem. Eng. J. 168 (2011) 731–736, https://doi.org/10.1016/j.cej.2011.01.068.
[199] K. Wang, Y.J. Wang, G.G. Chen, G.S. Luo, J.D. Wang, Enhancement of mixing and mass transfer performance with a microstructure minireactor for controllable preparation of $CaCO_3$ nanoparticles, Ind. Eng. Chem. Res. 46 (2007) 6092–6098, https://doi.org/10.1021/ie061502+.
[200] J.A.M. Van der Houwen, G. Cressey, B.A. Cressey, E. Valsami-Jones, The effect of organic ligands on the crystallinity of calcium phosphate, J. Cryst. Growth 249 (2003) 572–583, https://doi.org/10.1016/S0022-0248(02)02227-3.
[201] X. Wei, C. Shen, Y. Sun, W. Yi, Characteristic of the organic carbon-isotope composition and contribution of suspended matter in the Pearl River, Sci. Geogr. Sin. 23 (2003) 471–476.
[202] T. Beuvier, B. Calvignac, G.J.R. Delcroix, M.K. Tran, S. Kodjikian, N. Delorme, J.F. Bardeau, A. Gibaud, F. Boury, Synthesis of hollow vaterite $CaCO_3$ microspheres in supercritical carbon dioxide medium, J. Mater. Chem. 21 (2011) 9757–9761, https://doi.org/10.1039/c1jm10770d.
[203] X. Guan, F. Huang, J. Li, S. Li, X. Zhang, D. Guo, Y. Shen, A. Xie, Morphology control and mechanisms of $CaCO_3$ crystallization on gas - liquid interfaces of CO_2/NH_3 bubbles in aqueons-glycine solutions, Russ. J. Phys. Chem. A 89 (2015) 1091–1095, https://doi.org/10.1134/S0036024415060333.
[204] S.F. Chen, S.H. Yu, J. Hang, F. Li, Y. Liu, Polymorph discrimination of $CaCO_3$ mineral in an ethanol/water solution: formation of complex vaterite superstructures and aragonite rods, Chem. Mater. 18 (2006) 115–122, https://doi.org/10.1021/cm0519028.
[205] T.J. Lee, S.J. Hong, J.Y. Park, H.J. Kim, Effects of anionic polyacrylamide on carbonation for the crystallization of precipitated calcium carbonate, Cryst. Growth Des. 15 (2015) 1652–1657, https://doi.org/10.1021/cg501419e.
[206] L. Xiang, Y. Xiang, Z.G. Wang, Y. Jin, Influence of chemical additives on the formation of super-fine calcium carbonate, Powder Technol. 126 (2002) 129–133, https://doi.org/10.1016/S0032-5910(02)00047-5.
[207] J. Jiang, J. Liu, C. Liu, G. Zhang, X. Gong, J. Liu, Roles of oleic acid during micropore dispersing preparation of nano-calcium carbonate particles, Appl. Surf. Sci. 257 (2011) 7047–7053, https://doi.org/10.1016/j.apsusc.2011.03.001.
[208] C. Wang, X. Zhao, J. Zhao, Y. Liu, Y. Sheng, Z. Wang, Biomimetic nucleation and growth of hydrophobic vaterite nanoparticles with oleic acid in a methanol solution, Appl. Surf. Sci. 253 (2007) 4768–4772, https://doi.org/10.1016/j.apsusc.2006.10.048.
[209] A. Barhoum, H. Rahier, R.E. Abou-Zaied, M. Rehan, T. Dufour, G. Hill, A. Dufresne, Effect of cationic and anionic surfactants on the application of calcium carbonate nanoparticles in paper coating, ACS Appl. Mater. Interfaces 6 (2014) 2734–2744, https://doi.org/10.1021/am405278j.
[210] R. Agnihotri, S.K. Mahuli, S.S. Chauk, L.S. Fan, Influence of surface modifiers on the structure of precipitated calcium carbonate, Ind. Eng. Chem. Res. 38 (1999) 2283–2291, https://doi.org/10.1021/ie9900521.
[211] C. Zhang, J. Zhang, X. Feng, W. Li, Y. Zhao, B. Han, Influence of surfactants on the morphologies of $CaCO_3$ by carbonation route with compressed CO_2, Colloids Surf. A Physicochem. Eng. Asp. 324 (2008) 167–170, https://doi.org/10.1016/j.colsurfa.2008.04.010.
[212] Y. Sheng, B. Zhou, J. Zhao, N. Tao, K. Yu, Y. Tian, Z.C. Wang, Influence of octadecyl dihydrogen phosphate on the formation of active super-fine calcium carbonate, J. Colloid Interface Sci. 272 (2004) 326–329, https://doi.org/10.1016/j.jcis.2003.11.062.
[213] X. Chen, Y. Zhu, B. Zhou, Y. Guo, W. Gao, Y. Ma, S. Guan, L. Wang, Z. Wang, Hydrophilic $CaCO_3$ nanoparticles designed for poly (ethylene terephthalate), Powder Technol. 204 (2010) 21–26, https://doi.org/10.1016/j.powtec.2010.07.002.
[214] X. Chen, Y. Zhu, Y. Guo, B. Zhou, X. Zhao, Y. Du, H. Lei, M. Li, Z. Wang, Carbonization synthesis of hydrophobic $CaCO_3$ at room temperature, Colloids Surf. A Physicochem. Eng. Asp. 353 (2010) 97–103, https://doi.org/10.1016/j.colsurfa.2009.10.029.
[215] F. Kang, D. Wang, Y. Pu, X.F. Zeng, J.X. Wang, J.F. Chen, Efficient preparation of monodisperse $CaCO_3$ nanoparticles as overbased nanodetergents in a high-gravity rotating packed bed reactor, Powder Technol. 325 (2018) 405–411, https://doi.org/10.1016/j.powtec.2017.11.036.
[216] Z. Chen, S. Xiao, F. Chen, D. Chen, J. Fang, M. Zhao, Calcium carbonate phase transformations during the carbonation reaction of calcium heavy alkylbenzene sulfonate overbased nanodetergents preparation, J. Colloid Interface Sci. 359 (2011) 56–67, https://doi.org/10.1016/j.jcis.2011.03.086.
[217] J. Chen, L. Shao, Mass production of nanoparticles by high gravity reactive precipitation technology with low cost, China Particuol. (2007)https://doi.org/10.1016/s1672-2515(07)60110-9.